## General Disclaimer

### One or more of the Following Statements may affect this Document

- This document has been reproduced from the best copy furnished by the organizational source. It is being released in the interest of making available as much information as possible.

- This document may contain data, which exceeds the sheet parameters. It was furnished in this condition by the organizational source and is the best copy available.

- This document may contain tone-on-tone or color graphs, charts and/or pictures, which have been reproduced in black and white.

- This document is paginated as submitted by the original source.

- Portions of this document are not fully legible due to the historical nature of some of the material. However, it is the best reproduction available from the original submission.

9950-742

ERD Line No. SE-6

DOE/JPL-955688-81/5
Distribution Category UC-63



# DEVELOPMENT OF AN ALL-METAL THICK FILM COST EFFECTIVE METALLIZATION SYSTEM FOR SOLAR CELLS

BERND ROSS
JOSEPH PARKER

BERND ROSS ASSOCIATES
2154 Blackmore Ct.
San Diego, CA 92109



INTERIM REPORT
May 1980 - Aug. 1981

July 1982

Contractual Acknowledgement

The JPL Low-Cost Silicon Solar Array Project is sponsored by the U.S. Department of Energy and forms part of the Solar Photovoltaic Conversion Program to initiate a major effort toward the development of low-cost solar arrays. This work was performed for the Jet Propulsion Laboratory, California Institute of Technology by agreement between NASA and DOE.

DRD Line No. SE-6

DOE/JPL-955688-81/5
Distribution Category UC-63

# DEVELOPMENT OF AN ALL-METAL THICK FILM COST EFFECTIVE METALLIZATION SYSTEM FOR SOLAR CELLS

BERND ROSS
JOSEPH PARKER

BERND ROSS ASSOCIATES
2154 Blackmore Ct.
San Diego, CA 92109

INTERIM REPORT
May 1980 - Aug. 1981

July 1982

Contractual Acknowledgement

The JPL Low-Cost Silicon Solar Array Project is sponsored by the U.S. Department of Energy and forms part of the Solar Photovoltaic Conversion Program to initiate a major effort toward the development of low-cost solar arrays. This work was performed for the Jet Propulsion Laboratory, California Institute of Technology by agreement between NASA and DOE.

TABLE OF CONTENTS

LIST OF ILLUSTRATIONS

LIST OF TABLES

## 1.0 Summary

Copper pastes were prepared by the first subcontractor. Properties of these pastes did not reproduce earlier results in rheology and metallurgy. Electrodes made with pastes produced under the previous contract were analyzed and compared with the raw materials.

A needle-like structure was observed on the earlier electroded solar cells, and was identified as eutectic copper-silicon by electron probe Xray spectroscopy. The existence of this phase was thought to benefit electrical and metallurgical properties of the contact. Subsequently electrodes made from new material were also shown to contain this phase while simultaneously having poor adhesion.

A solar cell experiment including front contact experimentation was done. No electrical information was obtained due to inadequate contact adhesion.

Experiments were conducted with variations in paste parameters, firing conditions, including gas ambients, furnace furniture, silicon surface and others.

The Photovoltaic Solar Energy Conference was attended and a paper was presented. Semiconductor and solar cell research activities in Munich were visited and activities of mutual interest were discussed.

A liquid medium, intended to provide transport during the carbon fluoride decomposition was incorporated in the paste with promising results, resulting in better adhesion and surviving preliminary environmental tests. 2 x 2 cm solar

cells made with fluorocarbon activated copper electrodes and gave 7% AMI efficiency (without AR coating).

## 2.0 Introduction

The purpose of this study is to provide economical, improved thick film solar cell contacts for the high-volume production of low-cost silicon solar array modules for the LSA Project.

This work is based upon the concept of an all metal screenable electrode ink, investigated in Contract #955164. It was first found that silver powder with lead acting as a liquid sintering medium and with silver fluoride acting as an oxide scavenger, continuous adherent electrode layers result on silicon. During the final phase of the antecedent contract it was shown that base metals such as copper can likewise be sintered to provide an ohmic contact on silicon when appropriately doped. The most successful screened solar cell contacts were achieved using germanium-aluminum and silicon-aluminum eutectics as additions to the pastes for back contacts.

The objectives of the investigation are to provide all metal screenable pastes using economical base metals, suitable for application to low-to-high conductivity silicon of either conductivity type and possibly to aluminum surfaces.

## 3.0 Work With Earlier Copper Systems

### 3.1 Attempts to Reproduce S071, S079 and S080 Pastes

Pastes were prepared by the first subcontractor with silver fluoride obtained from several sources in order to determine the material giving optimum adhesion of fired contacts, and obtain properties reproducing earlier results[1,2]. Sources included Alfa Chemical Company, Apache Chemical and Hudson Labs. A batch of S071 (similar to F1, Table VI) prepared with silver fluoride left over from the previous contract did not give results distinguishable from the others.

The best paste in color and adhesion was S071A9 prepared with Hudson Laboratories silver fluoride. Fifteen different batches of S071 were tried.

The firing process was examined, and firing experiments were carried out in three different facilities: AVX Materials Division (forming gas consisting of 90% nitrogen and 10% hydrogen) in a belt furnace, Bernd Ross Associates, two step firing process (5 minutes nitrogen followed by 8 minutes of hydrogen) in a quartz tube furnace; Applied Solar Energy Corporation, similar two step firing process in a quartz tube furnace.

It was found that copper pastes prepared with silver fluoride exhibited a marked change in surface color as a function of time, independent of storage conditions. The surface changed from a reddish-brown color to dark brown and in extreme cases becoming almost black in appearance. Stirring immediately

restored the original color. Pastes containing all ingredients except silver fluoride did not exhibit a color change. While the effect of light upon silver halides is well known, this is not expected to be a factor, since pastes were kept in opaque glass containers. This phenomenon had not been observed with pastes prepared under the previous contract.

The sintering process appears to proceed in the recent pastes similarly to the previously fabricated material.

## 3.2 Results of Analysis

Figure 1 shows an SEM micrograph of paste S071-A18 in the dried, green (unfired) condition taken at 850X. Figure 2 shows the same ink printed on silicon and fired by the two-step process at 555°C, at the same magnification. Figure 3 is the same electrode at 4250X, both micrographs show good sintering action, denoted by grain growth and contiguous grain boundaries. Optical micrography was also used as an analytical tool. Figure 4 shows an optical micrograph of S079A3* fired at 500°C (two - step) at approximately 200X magnification. Figure 5 shows S071A10 fired at 550°C at the same magnification. Despite the higher temperature S071A10 appears to be more fine-grained. This may be due to the absence of the eutectic phase (aluminum-silicon) which lowers the system melting point of S079A3. Figure 6 shows the edge of a screened print of S071A9 fired at 550°C (two step) same magnification, and Figure 7 is similarly taken at the center of the electrode.

* similar to F1 with addition of 4wt.% Al-Si eutectic

Figure 8 shows a print under the same conditions except fired at a slightly higher temperature 575 $^{0}$ C. Since the magnifications are identical on all these micrographs, it is obvious that the 25$^{0}$ C temperature differential in the isochronal sintering experiment leads to significantly greater grain growth.

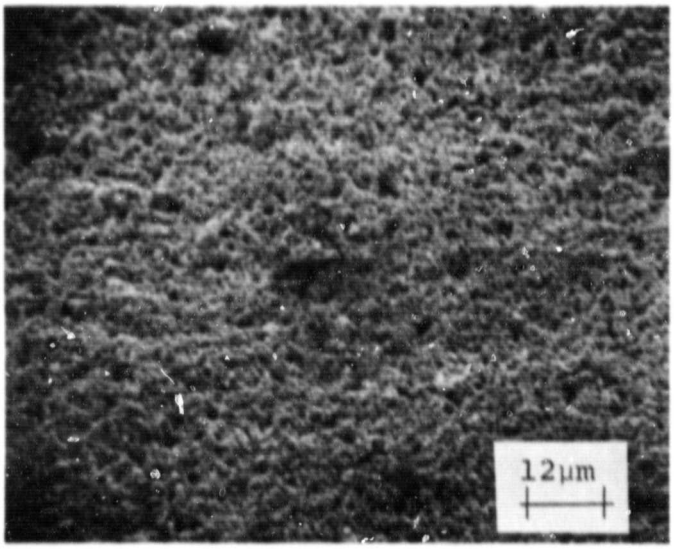


Fig. 1 SEM Micrograph of an unfired S071-A18 print, dried at 900°C, 850X.

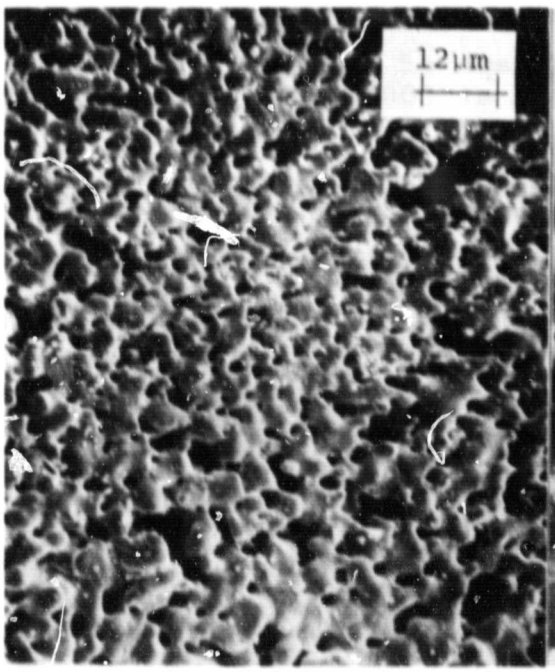


Fig. 2 Mag. 850X

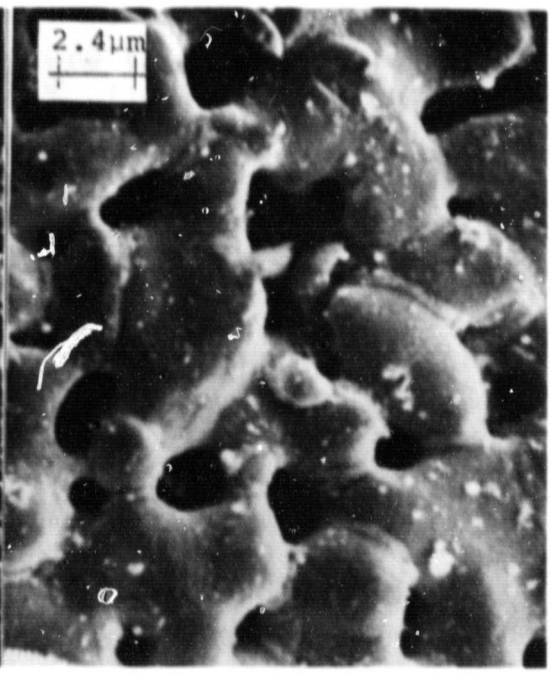


Fig. 3 Mag. 4250

SEM Micrograph of S071 print fired at 550°C by the nitrogen-hydrogen two step process.

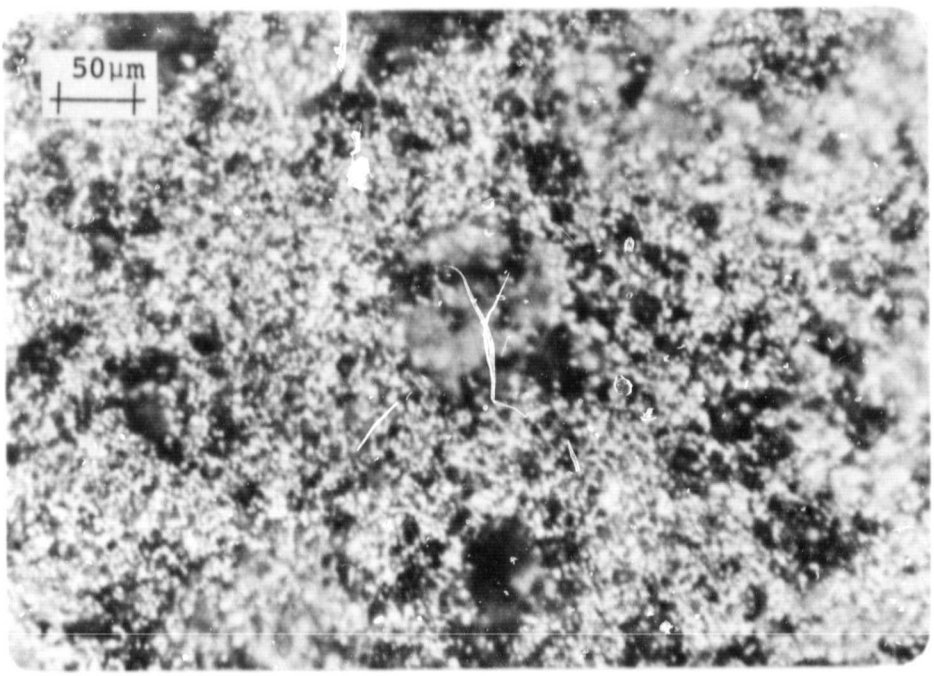


Fig. 4 Optical micrograph of S079A3 print (with eutectic dopant), fired at 500°C (two step) at 200X.

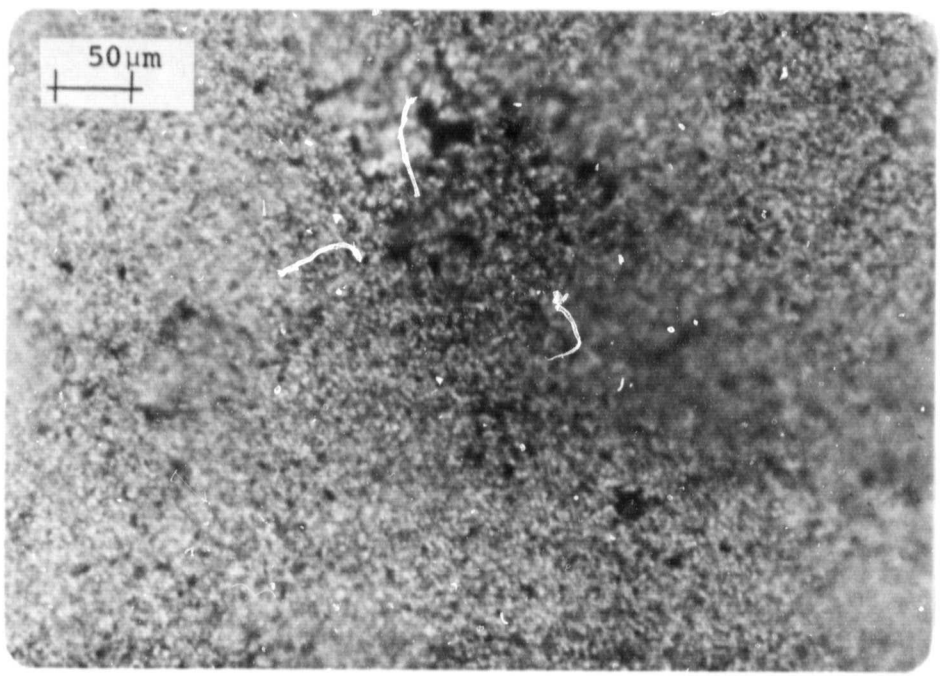


Fig. 5 Optical micrograph of S071A10 print (undoped) fired at 550°C (two step) at 200X.

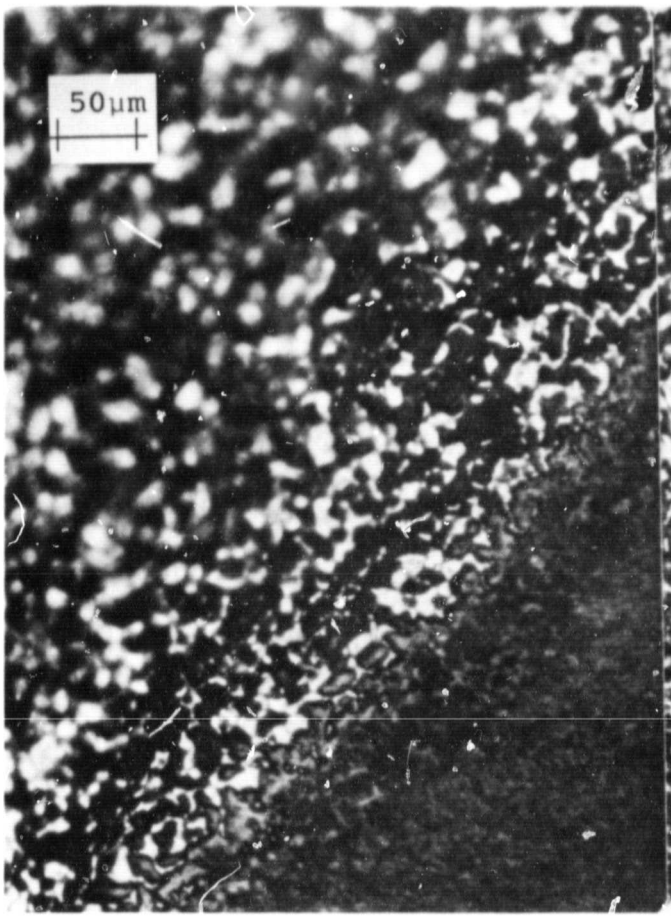


Fig. 6 Edge of print

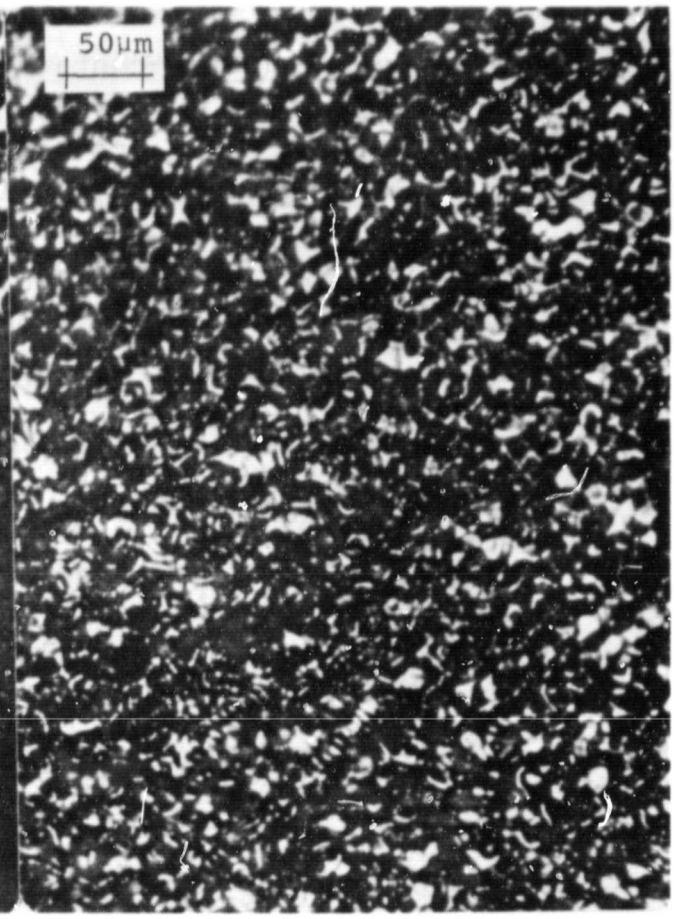


Fig. 7 Center of print

Optical micrograph of S071A9 fired at 550°C. Magnification 200X

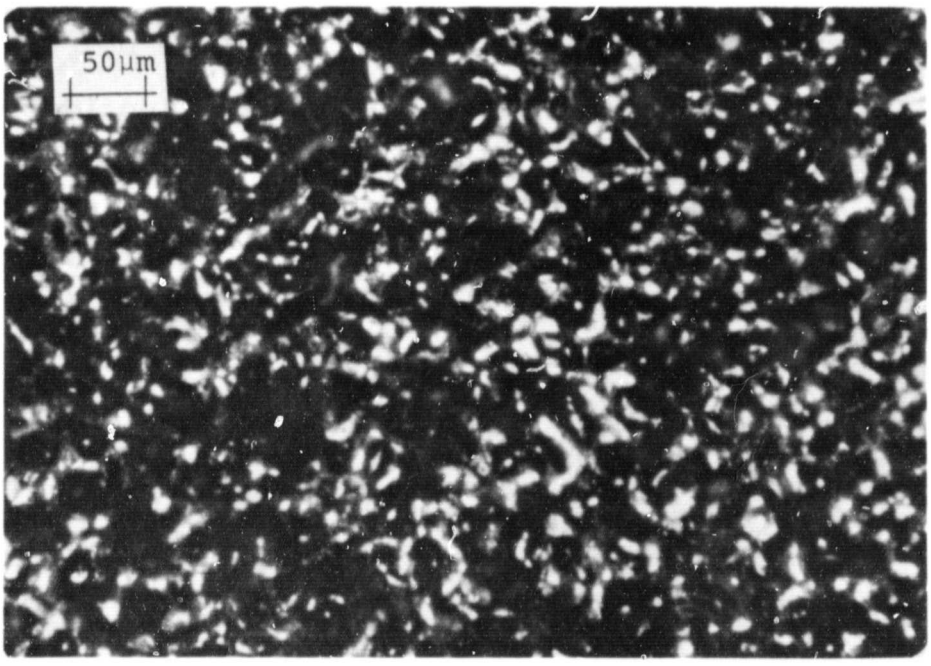


Fig. 8
Optical micrograph of S071A9 fired at 575°C.
Magnification 200X.

## 4.0 Silver fluoride-containing copper pastes

### 4.1 Paste and Contact Experimentation, Silver Fluoride

During the reporting period eleven pastes using fluorocarbon and eleven pastes using silver fluoride were fabricated. Most of these gave poor results, with powdery surfaces indicating inadequate sintering and insufficient adhesion. Figure 9 shows a macrophotograph of a number of test pieces of early electrode paste samples. The Scotch tape strip for the adhesion test is displayed above each sample. Pastes are from top to bottom F5 (AgF), F6 (AgF) and F7 (fluorocarbon) and the firing temperatures are from left to right 525°C, 550°C, 575 °C, 600 °C, and 625 °C. In some cases the total electrode lifted from the substrate.

Since adhesion of the copper silver fluoride pastes was so poor, it was decided to try some of the original silver pastes (containing 2% silver fluoride) which had given acceptable adhesion and scratch resistance. Silicon wafers were screened with silver ink S032 and fired at 550 °C in air and by the two step process. Excellent adhesion was obtained in the case of airfired silver electrodes. Silver electrodes fired in hydrogen separated from the substrates spontaneously. The silver electrodes removed from the substrates had good sheet integrity and strength.

The structure of the silver electrode sheets is shown in Figures 10 and 11 at 1800x and 9000x, respectively. The structure is so well interlocked as to appear oversintered. The smaller circular dots are believed to be a segregated metallic lead phase.

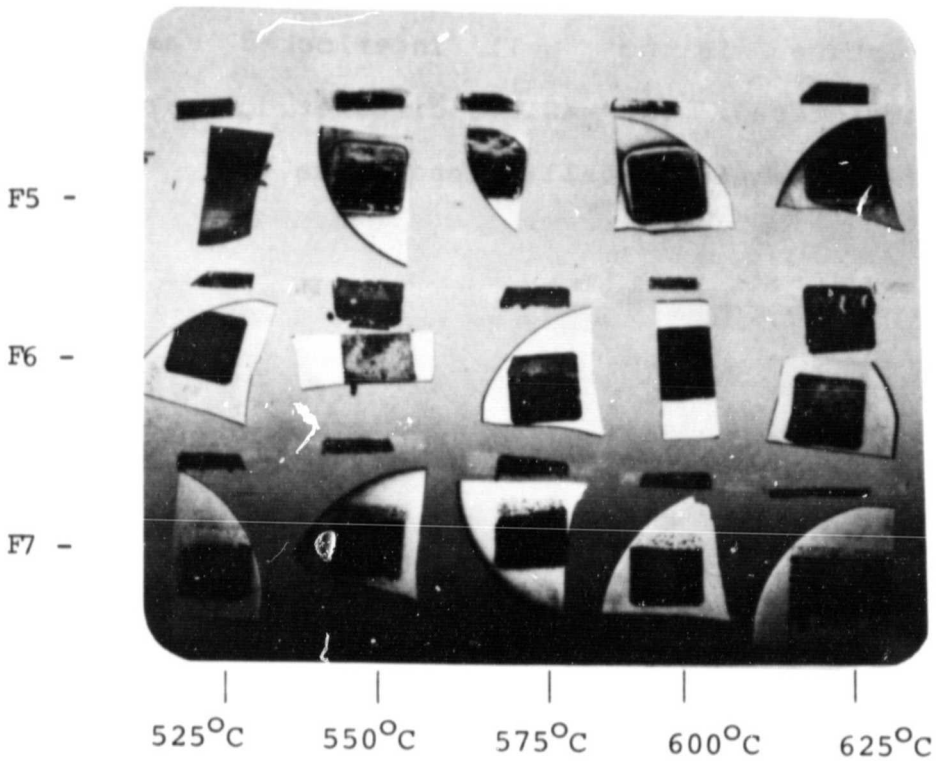


Figure 9. Photograph of 3 pastes with Scotch tape test strips above.

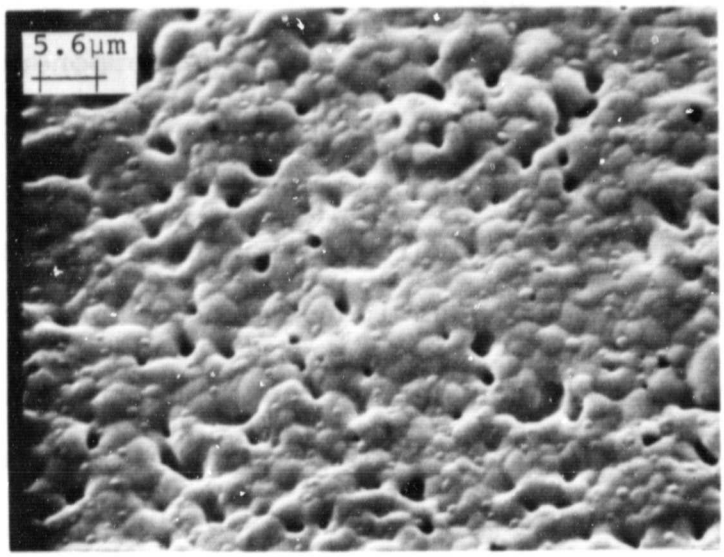


Figure 10 SEM micrograph of S032 silver electrode separated from silicon substrate, fired at 550°C by two step process at 1800x.

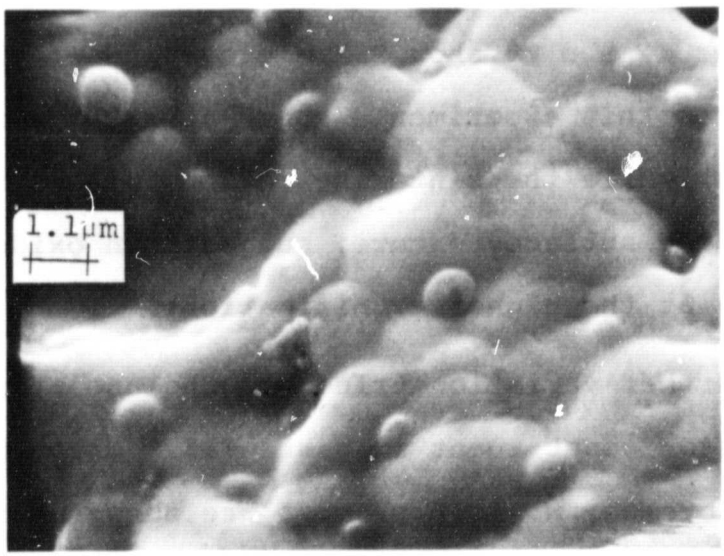


Figure 11 SEM micrograph of S032 silver electrode separated from silicon substrate, fired at 550°C by two step process at 9000x.

Previously we suspected interference of the hydrogen with the etching action of the fluorine component. In view of the information obtained in Section 8.0, another explanation may be in order. The bonds at the silicon surface may be more attractive to hydrogen than other atomic species, based upon the remarkable silicon-hydrogen bond strength.

Silver fluoride content of the copper pastes ranged from 1.1 wt% to 3.7 wt%. Smaller quantities of silver fluoride were utilized after an analysis by Dr. Joseph Parker, which pointed to spoiler reactions resulting from the presence of silver fluoride (Section 7.0).

The paste containing the smallest amount of silver fluoride gave the best results to date. One test sample fired in nitrogen at 550°C, passing the Scotch tape test (F12). Figures 12 and 13 show SEM micrographs of electrodes resulting from this experiment (shown at 1800x and 9000x, respectively) while the sintering action appears to be moderately good, the surface texture, suggests an oxide coating (particularly at the higher magnification).

One further variation tried was the use of copper flake for the major constituent in paste F15. Electrodes fired at 550°C by the two step process are shown as SEM micrographs in Figures 14 and 15. Magnifications are 1800x and 9000x, respectively. The electrodes resulting from this had good metallic sheen, presumably due to the orientation of the major flake plane, but poor adhesion and cohesion. In

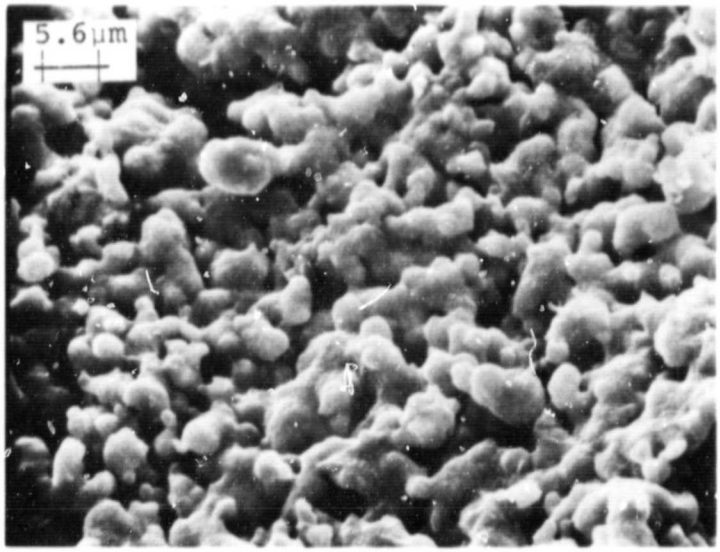


Figure 12 SEM micrograph of F12 electrode fired in nitrogen at 550°C, at 1800x.

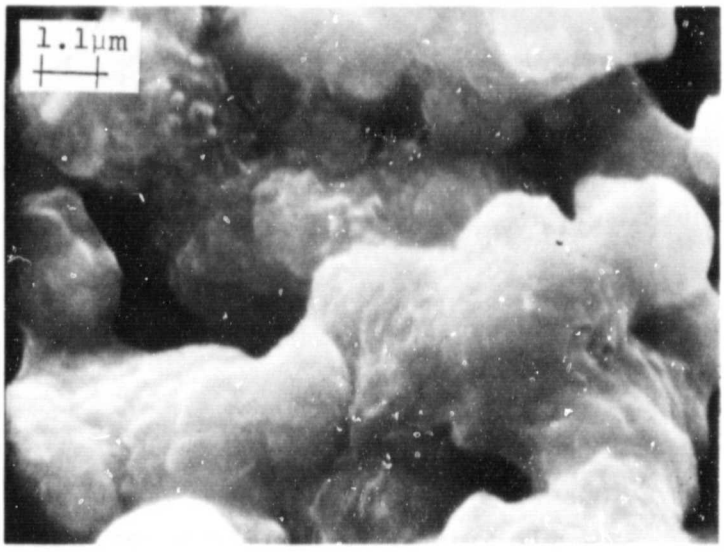


Figure 13 SEM micrograph of F12 electrode fired in nitrogen at 550°C, at 9000x.

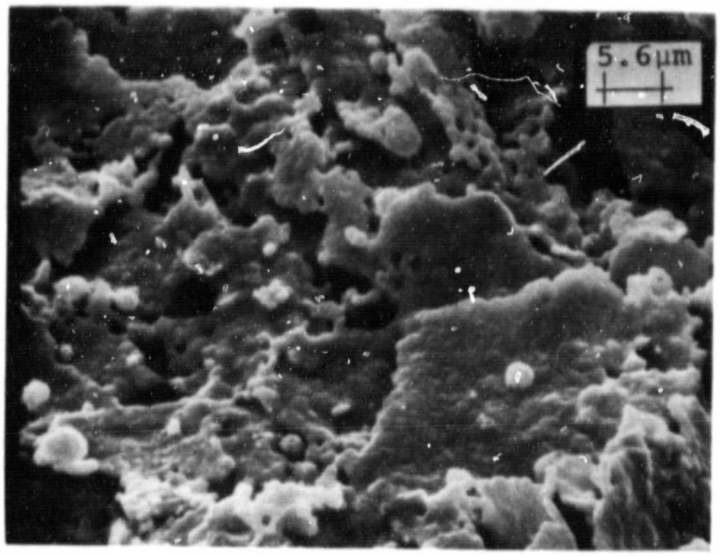


Figure 14 SEM micrograph of F15 copper paste with flake copper and silver fluoride, fired by the two step process at 550°C, at 1800x.

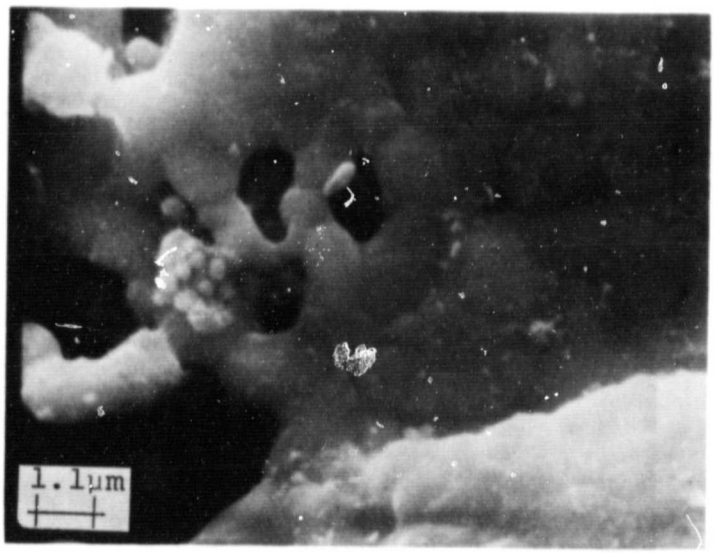


Figure 15 SEM micrograph of F15 copper paste with flake copper and silver fluoride, fired by the two step process at 550°C, at 9000x.

addition, the flakes tended to coat the screen wire mesh.

S080 electrodes fabricated during a solar cell experiment under the previous contract[3] were reexamined. A fragment of a solar cell which originally had a copper contact applied with initially good adhesion, was found to have the contact partially separated. The electrode metal was curved away from the silicon substrate, indicative of strain, in the sense of contraction relative to the silicon. This is as would be expected from the thermal behavior of copper relative to silicon. The thermal expansion coefficients of copper, lead and silicon are, respectively:

$$\text{Copper} \quad \frac{1}{L}\frac{\partial L}{\partial T} = 17.71 \cdot 10^{-6} \ (^{o}C)^{-1}$$

$$\text{Lead} \quad \frac{1}{L}\frac{\partial L}{\partial T} = 28.9 \cdot 10^{-6} \ (^{o}C)^{-1}$$

$$\text{Silicon} \quad \frac{1}{L}\frac{\partial L}{\partial T} = 2.56 \cdot 10^{-6} \ (^{o}C)^{-1}$$

If appropriately sintered, a copper grain matrix exists at the end of the sintering step, which took place at 550°C in the subject device. The amount of strain resulting from the mismatch is 0.05 cm. Assuming the diameter of the solar cell to be 2.25 inches or 5.72 cm and the copper grain matrix to cool through 520°C without relaxation, the calculated radius of curvature of the electrode is 45.5 cm.

While the initial adhesion of S080 paste was excellent it appears that longterm storage (approximately 18 months) caused catastrophic spalling of the copper electrode.

While the causes for this are not known, it may be that the relatively thick and densely sintered electrode could not withstand thermal cycling.

## 4.2 Solar Cell Experiments

The solar cell experiments were done with pastes SO71 and SO93 involving the front contact. The first of these utilized wafers with various junction depths and silicon oxide coatings. The experimental parameters were described in detail in reference 4. Due to poor adhesion no electrical data could be obtained.

In a second experiment, paste F20 was utilized on cells with a junction depth of approximately 0.5μm and an $SiO_2$ antireflection coating. As in the first experiment the contact was screened on the AR coating with the intent of firing through. The contact adhesion problem was again sufficient to prevent the taking of solar cell measurement data.

Results of Analysis

A simple Scotch[r] tape adherence test was devised to allow crude, instant evaluation of the results of electrode tests. Likewise a scratch test, that allows comparative analysis of the electrode strength, was initiated.

During the present reporting period a number of pastes manufactured previously with varying parameters were analyzed. The manual screening was improved to allow reproducible registration and constant snapoff distance (.012"). The tube furnace was reprofiled with the standard platinum - platinum plus 13% rhodium thermocouple and a digital microvoltmeter. An error was found on the furnace chromel-alumel thermocouple. Spot checks with platinum reference thermocouple were made routine on all firings. Some variation in firing was found leading to some suspicion of potential downstream contamination from contaminated furnace tube, gas or exudant from upstream samples.

Problems with layers were:

1) Lack of adhesion, possibly due to inadequate reduction of oxide, (silicon surface and powder grain surfaces) or tying up of dangling surface bonds by hydrogen atoms.
2) Poor sintering due to inadequate liquid transport (discussed in Section 5.1).

Samples of characterization attempts of successful and unsuccessful pastes are shown in the following figures. Figure 16 depicts four optical photomicrographs of successful S080 substrates (upper left) and S080 print (upper right) and unsuccessful S079 substrate (lower left)

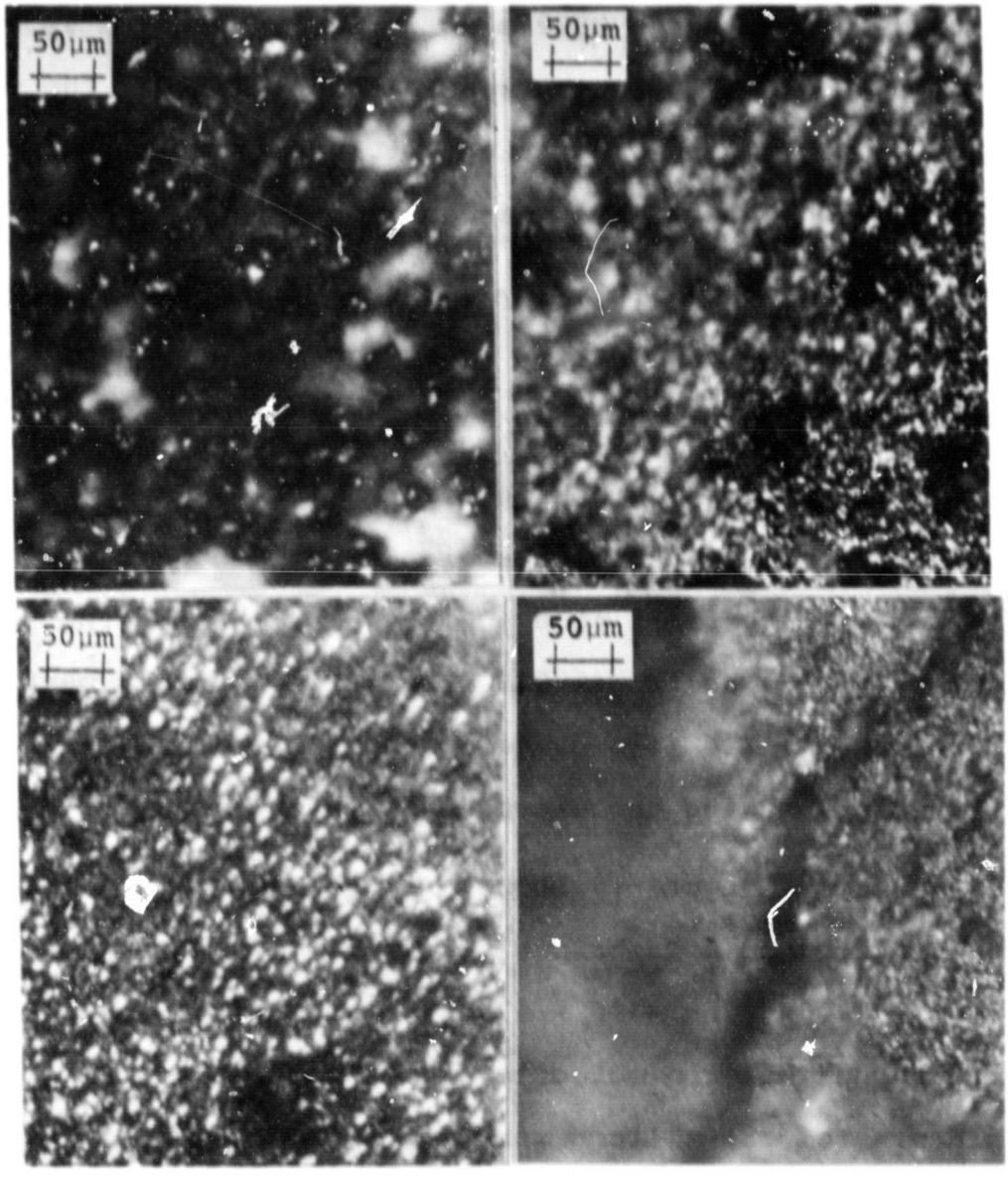


Figure 16 Optical micrographs of S080 successful and S079 unsuccessful screened prints with experimental copper pastes.
LEFT SIDE, TOP: Silicon substrate under good S080 print (electrode removed by acid etch).
BOTTOM: Silicon substrate of S079 print (electrode peeled spontaneously).
RIGHT SIDE, TOP: S080 successful electrode print.
BOTTOM: S079 unsuccessful electrode print.
Magnification 200X

and S079 print (lower right). In the case of the substrates the S080 electrode was removed by etching with concentrated nitric acid, and the S079 electrode print peeled spontaneously. The difference between S080 and S079 is the use of germanium-silicon eutectic at 5wt.% in the former and aluminum-silicon eutectic in the latter.

The major observable difference in the micrographs is the larger grain size and coarser faceting in the case of the successful S080 paste.

Figure 17 shows a composite of SEM micrographs depicting an unsuccessful S080 electroding experiment. The substrate is shown on the left side and the electrode on the right, both at 1800x and at 4500x. The firing of this paste at 550$^{o}$C by the two step process resulted in a small degree of sintering, making the micrograph resemble that of a powder.

By contrast, Figure 18 shows a successful print of the S080 paste taken on a Cambridge SEM at roughly two magnifications 1800 - 1900x, and 4500 - 4700x. The striking appearance of the copper silicon eutectic needle structure dominates the pictures of the silicon substrate. On the right the electrode can be seen.

Figures 19and 20 show black and white reproductions of the color readout of xray dispersive spectra of successful S080 electrodes and the silicon substrate, respectively. The spectra allow reading of the lines of copper (Cu), Aluminum

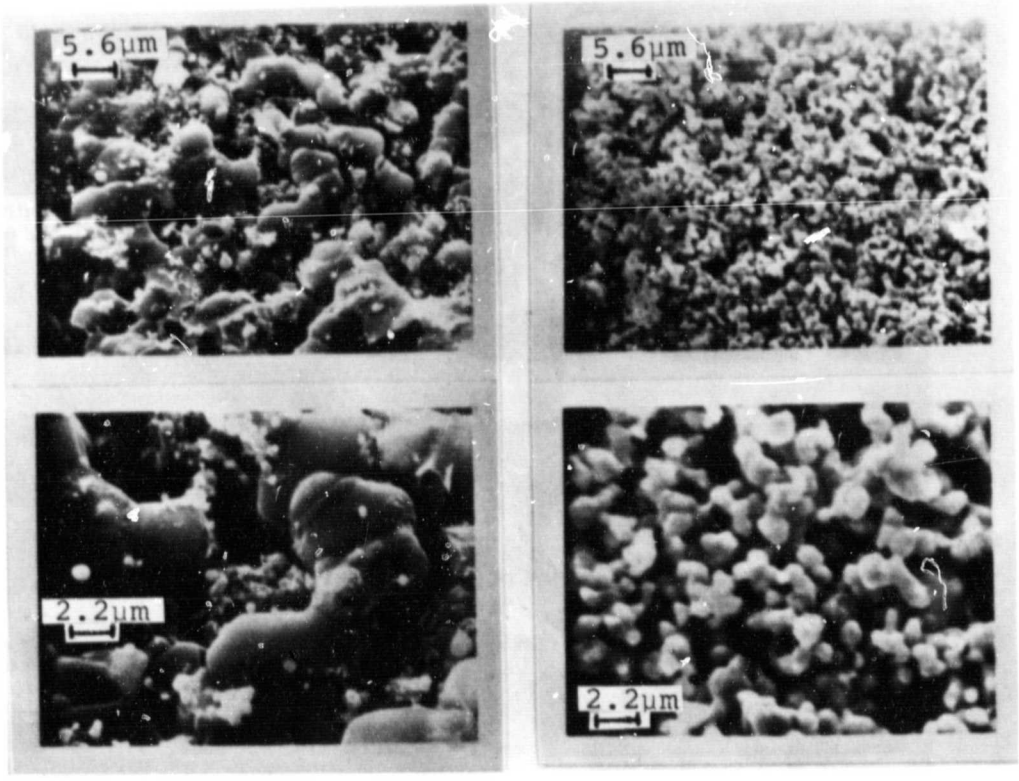


Figure 17 Composite of SEM micrographs of S080 unsuccessful electroding experiment.
Left Side: Substrate.
Right Side: Electrode.

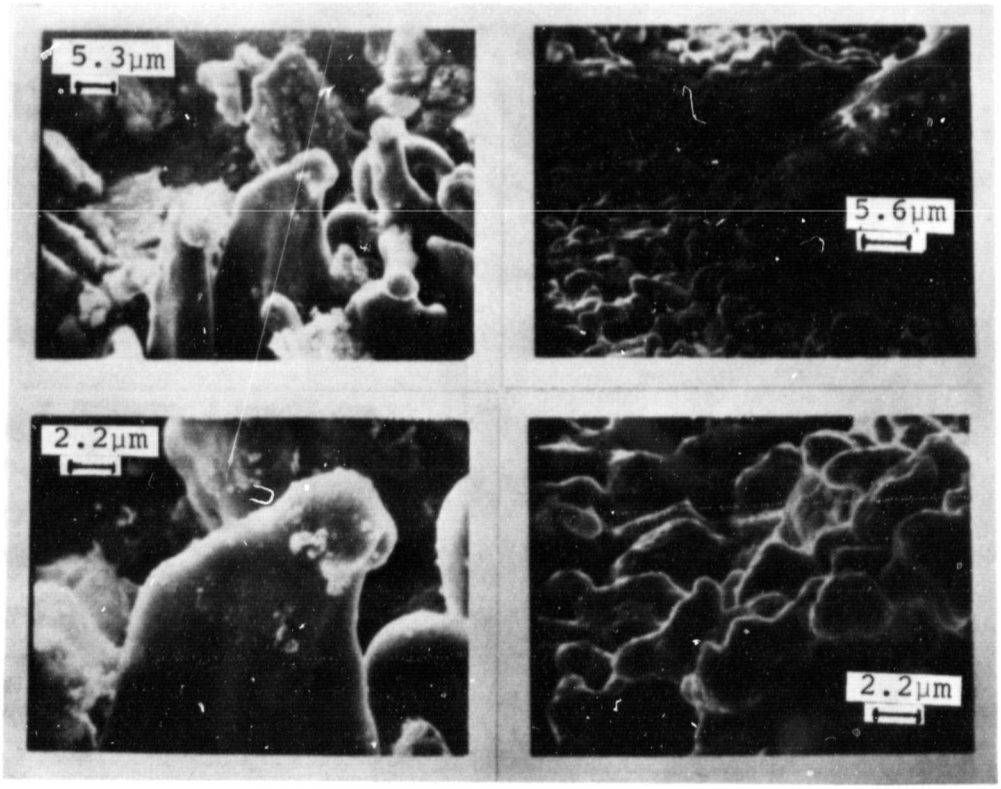


Figure 18 Composite of SEM micrographs of S080 successful screen print.
Left Side: Silicon substrate.
Right Side: Electrode.

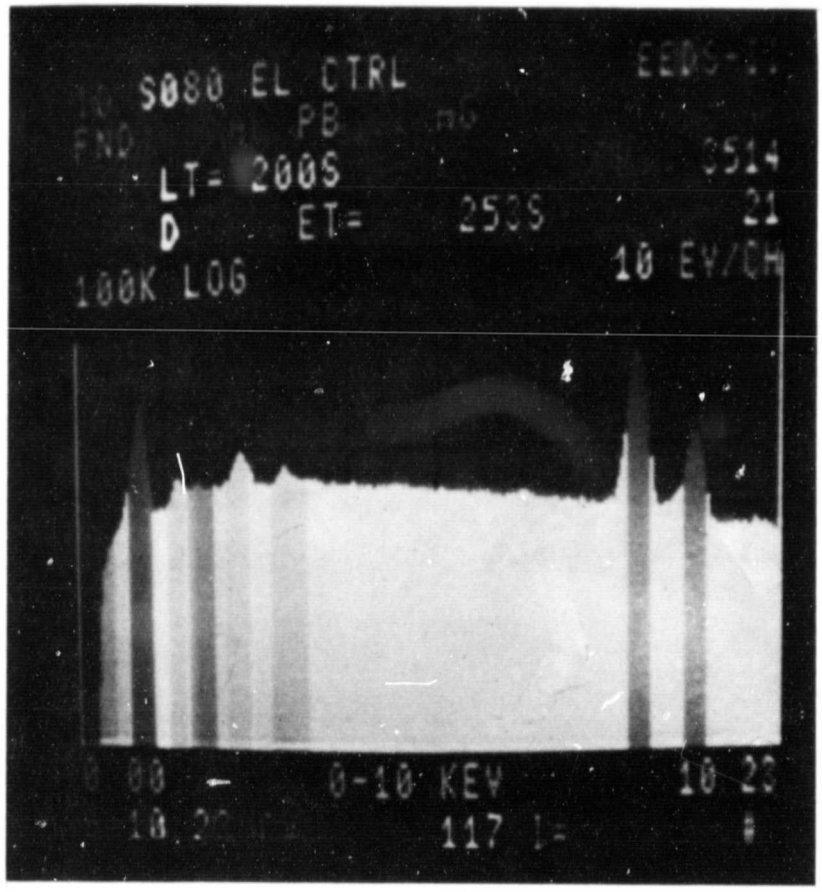


Figure 19 Black and white reproduction of color coded Xray dispersive spectrum of successful S080 electrode.

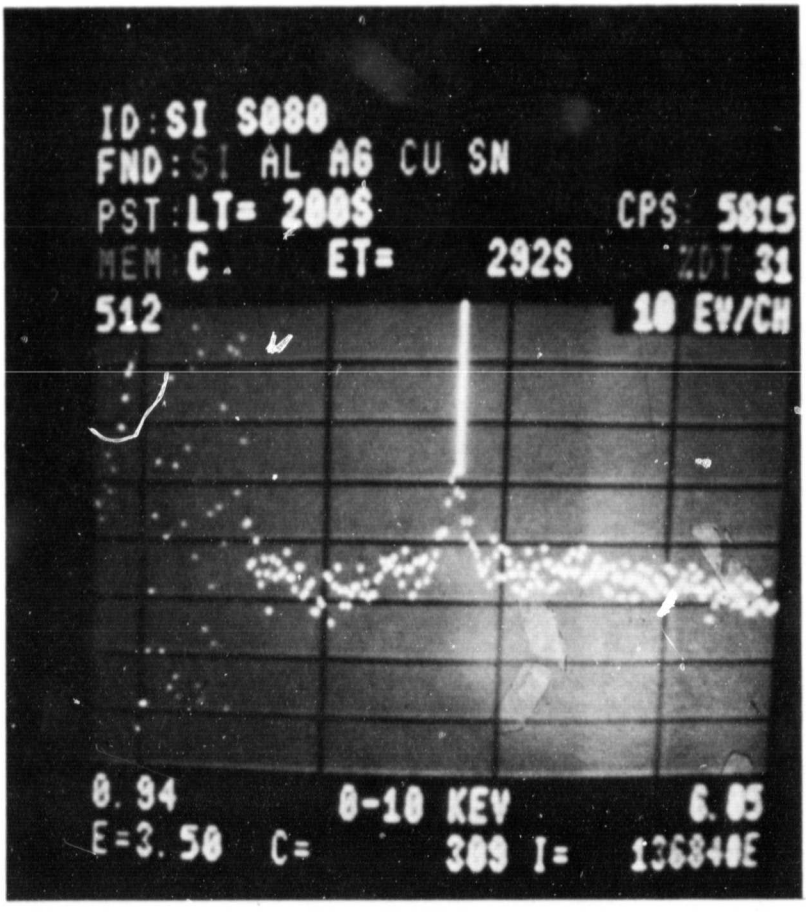


Figure 20 Black and white reproduction of color coded Xray dispersive spectrum of successful S080 electrode.

5.0 Cont.

(Al), lead (Pb) silicon (Si) and silver in Figure 19 and silicon, aluminum silver, copper and tin (Sn) in Figure 20 The figures are shown only as illustrative of the method, as no clues for the differences in performance could be obtained from the spectra.

## 5.0 Fluorocarbon containing copper pastes

### 5.1 Paste, Contact Experiments and Analysis

During the present interval paste formulation was reinstated at a new subcontract facility. The purpose of this change was to allow more intimate control of material and process by direct contract personnel.

New screens were designed and fabricated in order to allow utilization of convenient and economical 2cm x 2cm solar cell blanks. A design was made for a universal test pattern and solar cell front and back electrodes. These could be used both for basic ink parameter measurements and solar cell contact experimentation. The test pattern allows measurement of contact resistance, line resistance substrate resistivity, optical line resolution and electrical line resolution and is shown in Figure 21. The linear pattern at the top facilitates a measurement allowing the calculation of contact resistivity (in $\Omega cm^2$), simultaneously giving the resistivity of the silicon substrate. The large squares (2.5mm x 2.5mm), at the extremes of the linear array, provide the current electrodes in the measurement, while the small series of rectangles provide the voltage sources in the array. This portion of the design had been used previously[5]. A long line at the periphery of the pattern was used for measurement of the electrode resistance, from which the electrode resistivity can be calculated by

(1) $$\rho = R \frac{tw}{\ell} \Omega cm$$

where $\rho \equiv$ electrode resistivity $\Omega cm$
$R \equiv$ measured resistance, $\Omega$
$t \equiv$ electrode thickness, cm
$w \equiv$ electrode width, cm
$\ell \equiv$ electrode length, cm

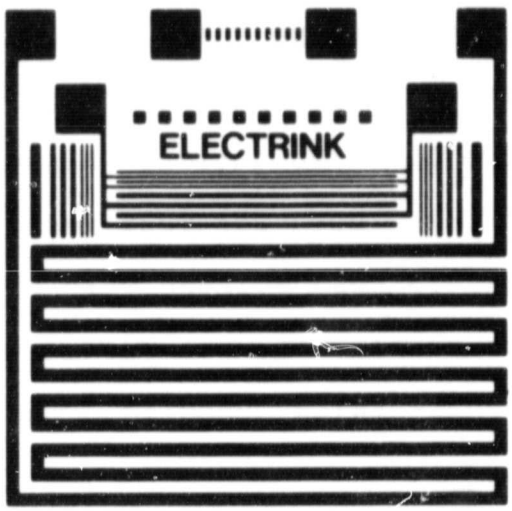


3X Actual Size

Figure 21 Photograph of screen pattern, with contact resistance, line resistance optical and electrical resolution test.

The interwoven pattern under the contact resistance array serves to determine line definition and the degree of measurable crossover or bridging, based upon a resistance measurement. It will be noted that two sets of line pairs are provided, one that is coarse (.009 inches line width and spacing) and one that is fine, .004 inches line width and spacing (See Figure 21, lower and upper portion, respectively). It has been noted that screening in a direction perpendicular to a line tends to reduce line resolution. Based upon these designs, frames were ordered both for #325 mesh screens and #230 mesh screens. The #325 mesh screens were chosen initially to allow ultimate resolution, but proved to be too fine to allow sufficiently thick deposits. The #230 mesh screens were adequate.

Initial experiments with fluorocarbon pastes gave unsatisfactory results, both from an adhesive and a sintering standpoint. Figures 22 and 23 show an example of an electrode which exemplifies the problem. Microscopic examination of the lead raw material showed that a high percentage of the grains were quite large (~50μm), resulting both in poor distribution of the liquid sintering medium, as well as the possibility of the printing screen acting as a sieve. This would hold back a portion of the lead component, upsetting the intended compositional ratios, and could explain the problem of undersintering.

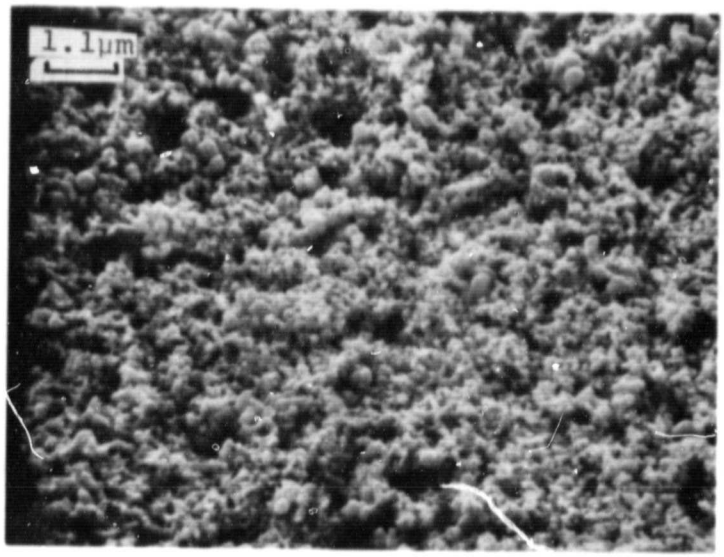


Figure 22 SEM micrograph at 1800x of F7 copper fluorocarbon paste fired at 600°C by the two step process.

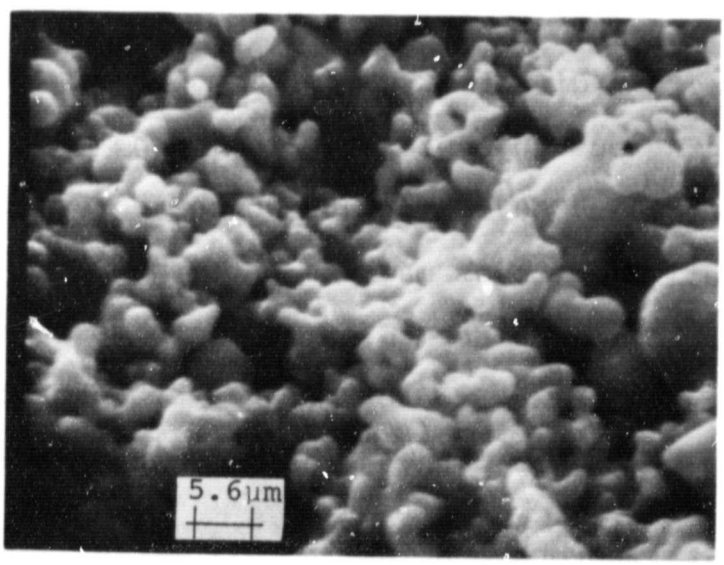


Figure 23 Same as above except 9000x. Note lack of sintering as shown by small particle size and absence of contiguous grain aggregates.

This problem was eliminated by ordering #200 lead powder, and sifting the available powder through a #400 stainless steel screen. Some improvement in sintering resulted from this procedure, however the adhesion problem remained.

In addition to problems with excessive particle size in lead, copper powder from suppliers other than Colonial Metal Corporation also had too large a particle size distribution (large particle diameters). However, the most recent batch of copper received from Colonial Metals Corporation was below specifications for particle size and gave problems with a) the amount of powder that could be accommodated by a given quantity of vehicle (metal content) and b) the apparent "fluffiness" of the metal powder. Both a) and b) are attributable to smaller than usual particle diameters.

A total of 99 different paste formulations were manufactured by the previous subcontractor, including many attempts to reproduce S071, S079 and S080 which represented the best solar cell electrodes made to date (previous contract #955164)[6]. It was deemed appropriate to start over numbering pastes manufactured by the new subcontractor, beginning with F1 (which would have been S100 under the old scheme).

The first fluorocarbon ink in this series was F4 utilizing 0.7 wt% fluorocarbon powder with the results described above.

Pastes were produced with various copper powders including copper flake (see section 4.1 ), without a marked improvement. Fluorocarbon content was varied from 0.7 wt% (F4) to 2.1 wt% (F11) with the medium range (1.0 to 1.2 wt%) yielding the best results.

An extensive analysis was undertaken by Dr. Joseph Parker, of the possible chemical reactions of the paste constituents throughout the thermal history of the screened electrodes. A set of simple equations was written and the thermochemical analysis was done, based upon heats of reaction from published or derived heats of formation, for the various compounds. The numerical value and algebraic signs of the heats of formation indicate the likelihood that certain reactions are emphasized or reduced in quantity. Subsequently it was desirable to verify these clues by direct experimentation and further physical analysis with differential thermal analysis (DTA) and thermal gravimetric analysis (TGA) (see section 7.0).

The above analysis showed that it would be desirable to provide an additional liquid medium, whose function was to promote contact between the copper powder grains and the freshly exposed silicon surface, during the scavenging activity of the fluorine from the fluorocarbon source. Earlier work with silver fluoride had shown that the fluorine scavenging activity takes place very rapidly (~1 sec), while the silver fluoride salt is in a liquid form. The reaction

products, solid silver metal and gaseous silicon tetrafluoride, as well as water, drive the reversible reaction in one direction through the mass action law, and the contact between silver and silicon is a consequence of the reaction site. Contact between the copper grains and the silver fluoride is promoted by the liquid lead (liquid phase sintering medium), during the longer term of the sintering step. In the case of the fluorocarbon decomposition the reaction proceeds without the presence of sufficient liquid phase, making the contact between copper and freshly exposed silicon less probable. This is because the amount of fluorocarbon has to be kept low due to other potential spoiler reactions and due to the low density of fluorocarbon making it a nonideal transport medium. An additional liquid medium, lead acetate, melting point 280°C, was therefore chosen to transport copper grains to freshly exposed silicon sites. Liquid sintering of the copper matrix is still thought to be a solution growth phenomenon accomplished by the liquid metal lead.

The first paste containing lead acetate and fluorocarbon powder was F13 copper paste. The composition of this paste is given in Table 1 below.

Table 1 Composition of Paste F13

| Material | Source | Amount (wt%) |
|---|---|---|
| Vehicle | Dupont | 34.0 |
| Fluorocarbon | Dupont | 1.1 |
| Aluminum-Silicon eutectic | Alfa-Ventron | 1.1 |
| Lead Acetate | Bakers | 2.3 |
| Lead Metal | MCB | 4.6 |
| Copper Metal | Colonial | 56.9 |

The paste was screened as a test pattern as well as solid electrode. During firing at a temperature of 556°C several variations of gas ambients were tried. The normal nitrogen-hydrogen two step firing gave reasonably good adherence, although some pulloff was observed in the Scotch tape test.

The two step firing process was described previously[7], but will be repeated in Table II for the sake of completeness.

Table II Two Step Firing Process

| Time (minutes) | Gas | Wafer Temperature and Location |
|---|---|---|
| 10 | Nitrogen | ∿25°C (Room temperature) outside furnace |
| 3 | Nitrogen | 80°C - 150°C (dry) at furnace entrance |
| 5 | Nitrogen | at temperature (∿550°C) in furnace |
| 8 | Hydrogen | at temperature (∿550°C) in furnace |
| 2 | Hydrogen | 550°C → 25°C (slow cool) to furnace exit |
| 5 | Hydrogen | Cool outside furnace |
| 5 | Nitrogen | Cool outside furnace |

Best results were obtained in a run in which the sintering took place in nitrogen and hydrogen was used only during the cooling phase. A Scotch tape test (See Section 4.3 performed on the electrode from this run gave good results with virtually no pulloff.

Figure 24 and 25 show SEM micrographs of F13 electrodes fired at 550°C by the hydrogen cool process, with indicated magnifications. It can be seen that the degree of sintering is inadequate, and there is some evidence of oxidation in Figure 25 The two conditions may be related in that the lack of sintering may be due to lack of wetting by the liquid phase sintering

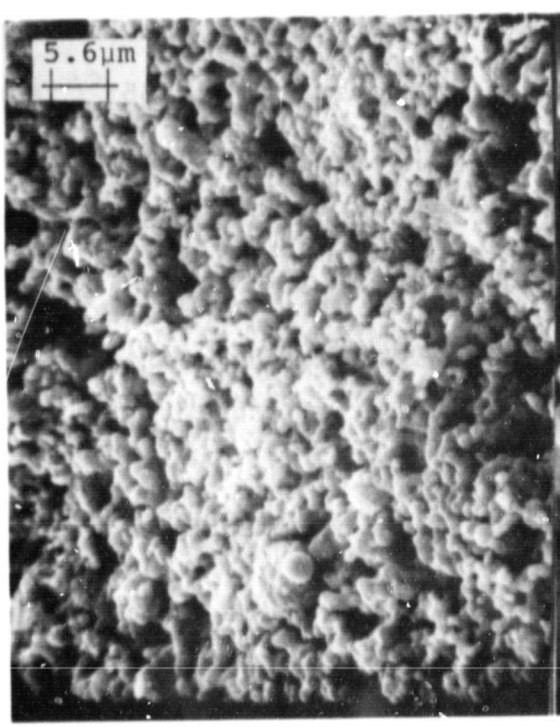


Figure 24 1800x

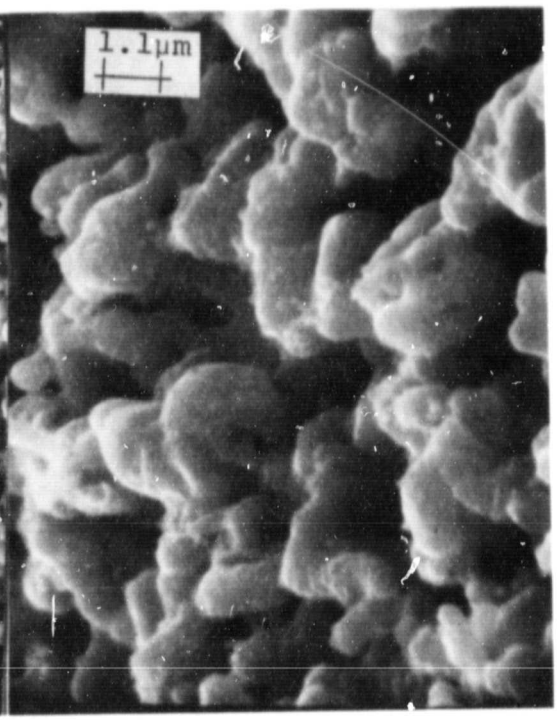


Figure 25 9000x

SEM micrographs of F13, copper fluorocarbon electrode.

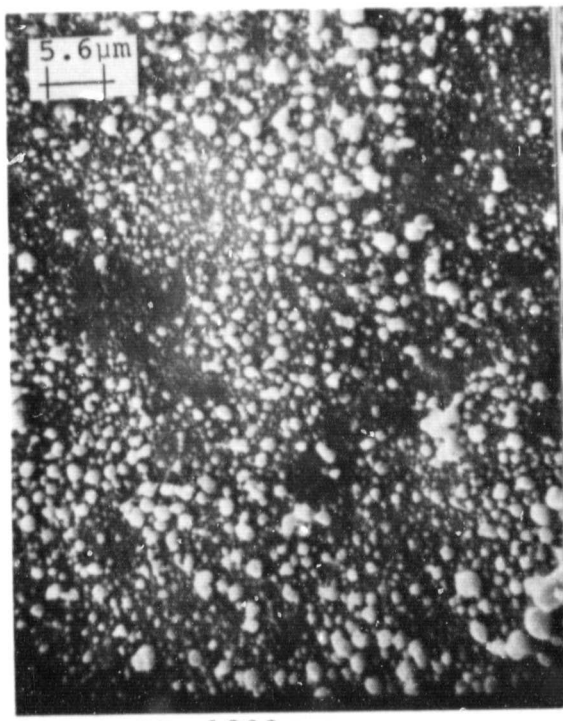


Figure 26 1800x

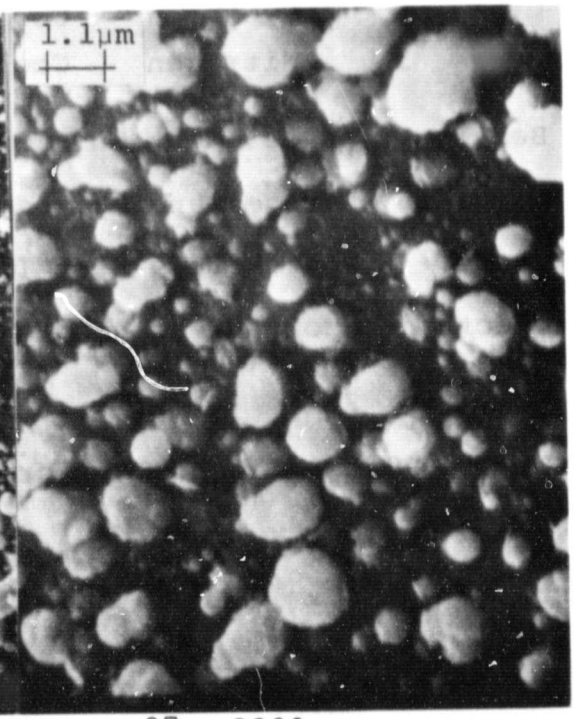


Figure 27 9000x

SEM micrographs of substrates under above electrodes.

medium (lead), since hydrogen is introduced only during cool-down. Figure 26 and 27 show SEM micrographs taken of substrates under F13 electrodes (525$^{o}$C) after electrodes were removed mechanically. The white beads covering the surface appear to be dielectric in nature judging from the presumed charging effects of Figure 27 Therefore we believe the material to have resulted from the lead acetate and expect it to be lead oxide.

## 5.2 Solar Cell Experiments

Screening experiment with F13, 16, 17 and F20 paste was made on 2 X 2 cm phosphorus diffused laser scribed and broken solar cell material. The back contact only was provided with a screened electrode of the above pastes. The specimens were fired by the normal two step procedure at 575°C and 625°C. The results were variable with most specimens failing the Scotch tape test. One device (not tape tested) was transmitted to the Jet Propulsion Lab for application of front contacts (Ti-Pd-Ag) and measurement.

The IV curve is shown in figure 28 The curve is characteristic of poor series and shunt resistance. An attempt to etch the cell edge to increase shunt resistance resulted in some improvement in open circuit voltage but simultaneously increased the series resistance, presumably as the cell mask (tape) was removed. While the device electrode (F16 screened paste) is far from optimized, it is an indication that the flouorocarbon containing paste is viable for solar cell electrodes. The uncoated solar cell had an efficiency of 7.0% initially (corresponding to 9.6% AM1 with AR coating).

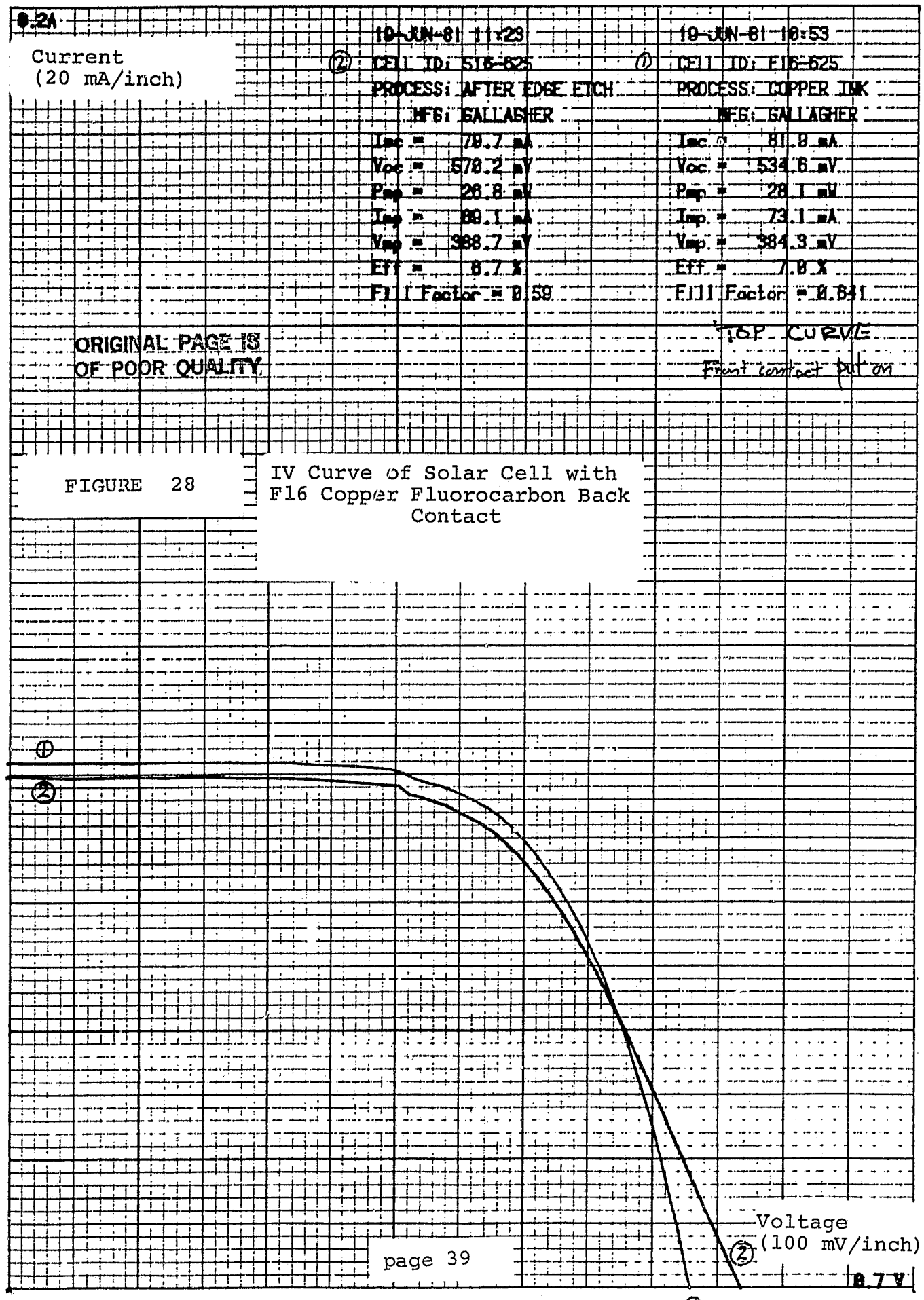


FIGURE 28

IV Curve of Solar Cell with F16 Copper Fluorocarbon Back Contact

## 6.0 Front Contact Considerations

### 6.1 Theory

The front contact of modern solar cells is applied to nearly degenerate n type semiconductor surfaces with impurity concentrations from $10^{19}$ atoms/cm$^{-3}$ to $10^{21}$ atoms/cm$^{-3}$ with phosphorous being the donor conventionally in use. Due to the high surface concentration and resulting high conductivity in accordance with

(1) $\sigma = Nq\mu$

where $\sigma$ = conductivity $(\Omega\ cm)^{-1}$

$N$ = carrier concentration, $cm^{-3}$

$q$ = electronic charge, coulombs

$\mu$ = mobility, $cm^2/V - sec$

it is relatively simple to provide a good ohmic contact to the front surface of solar cells. This results from the fact that the electron tunneling probability is a function of the carrier concentration on both sides of the interface. When a metal coats the surface of a semiconductor, the depletion width within the semiconductor shrinks as a function of carrier concentration, thereby enhancing the tunneling probability. An enhanced tunneling probability provides for ready carrier flow through the barrier constituted by the contact potential between contact metal and semiconductor surface.

The depletion width, W, can be calculated from

(2) $W = \sqrt{\frac{2\varepsilon_s}{qN_{D,A}}(V_R + V_D - \frac{kT}{q})}$ cm Ref 7

where $\varepsilon_s$ = permittivity of the semiconductor $1.06 \cdot 10^{-12}$ F/cm
$q$ = electronic charge, $1.6 \cdot 10^{-19}$ Coulomb
$N_D$ = donor concentrations, $1 \cdot 10^{20}$ $cm^{-3}$
$N_A$ = acceptor concentration, $5 \cdot 10^{19}$ $cm^{-3}$
$V_R$ = applied bias voltage, $V_R = 0$
(3) $V_D$ = $\phi_B - \phi_n$ = contact potential
$\phi_{BN}$ = copper - semiconductor barrier = 0.69eV Ref 8
$\phi_{BP}$ = 0.46eV Ref 8
(4) $\phi_n$ = $E_C - E_F$ = 0.0326eV
$\phi_p$ = $E_F - E_V$ = 0.0452eV
(5) $E_C$ = Conduction band edge potential, eV
$E_F$ = Fermi energy, eV
$k$ = Boltzmann constant J/°K
$T$ = Absolute Temperature °K

The depletion width of the front contact is

$W = 29.5$ Å

in the silicon.
The maximum field $\varepsilon_m$ is given by

(6) $\varepsilon_m = \sqrt{\frac{2qN_{D,A}}{\varepsilon_s}(V_R + V_D - \frac{kT}{q})} = 4.38 \cdot 10^6$ V/cm Ref 7

The contact resistivity can be calculated from the tunneling conductance

(7) $R_c = G_o^{-1} = \frac{W}{\sqrt{2m^*\phi}} (\frac{h}{q})^2 \exp \frac{4\pi W}{h}\sqrt{2m^*\phi}$ Ref 9

(8) $= 3.16 \cdot 10^{-11} \frac{W_o}{\sqrt{m^*/m\phi}} \exp 1.025 W_o \sqrt{m^*/m\ \phi}$

where $h$ = Planck's constant
$(m^*/m)_e$ = 0.1905 the effective electronic mass in the <100> direction

(9) $(m^*/m)_h$ = 0.16 the effective hole mass in the <100> direction
$\phi$ = $E_g - \phi_B$ = 0.42eV
$E_g$ = Energy gap of silicon = 1.11eV
Germanium = 0.65ev
$W$ = Depletion width in Angstroms

The calculated front contact tunneling resistance is

$$R_C = 1.69\ 10^{-5}\Omega cm^2$$

Since the barrier voltage values vary among workers, and their magnitude affects the argument of the exponent in equations 7, & 8, the calculated contact resistance is subject to wide variations.

Similiarly, the carrier concentration at specific depths and at the front surface is difficult to obtain precisely. The uncertainties in barrier voltage can result in depletion widths varying by a factor of two or more, giving tunneling resistances differing by three orders of magnitude. Figure 29 shows the variation of tunneling resistance as a function of barrier (or depletion) thickness.

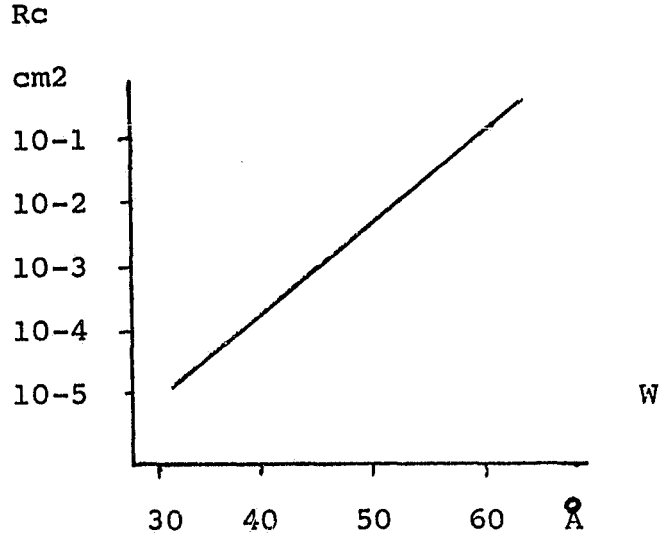


FIG 29 Contact tunneling resistance versus depletion width W

The depletion width for a copper contact to a backsurface field cell ($N_A = 5 \cdot 10^{18}$ Al/cm$^3$) is 105 Ångstroms, yielding a calculated tunneling contact resistance of $1.14 \cdot 10^{7}\ \Omega cm^2$.

The energy band relationships for a copper contact on a silicon front surface doped with $1 \cdot 10^{20}$ phosphorus atoms/$cm^3$ are shown in Figure 30 using the values calculated above. For the sake of completeness an energy band diagram is included in Figure 31 depicting the back contact relationships for a BSF cell, or a copper contact containing eutectic aluminum-silicon additive. For the case of aluminum-germanium (S080) a hetero-epitaxial situation exists, leading to a smaller band gap on the semiconductor side of the contact ($E_G$ (germanium) = 0.65eV).

For the case of a germanium-aluminum contact alloy on the cell backsurface the redeposition of aluminum doped germanium on the silicon leads to a narrower depletion width of 23.2 Angstroms due to a higher carrier concentration ($N_A = 1.3 \cdot 10^{20}$ Al/$cm^3$) and smaller barrier height of 0.42 eV. The effective mass of the hole is also considerably smaller in germanium ($\frac{m^*}{m} = 0.042$). This leads to a tunneling resistance of $7.5 \cdot 10^{-8}$ ohm-$cm^2$.

When the semiconductor surface has a higher resistivity, it may be necessary to make special provisions in applying the ohmic contact by utilizing a technique to dope the surface of the semiconductor under the electrode metal. When firing temperatures are sufficiently high ($\gtrsim 800^{\circ}C$) this may be done by including an elemental donor impurity in the

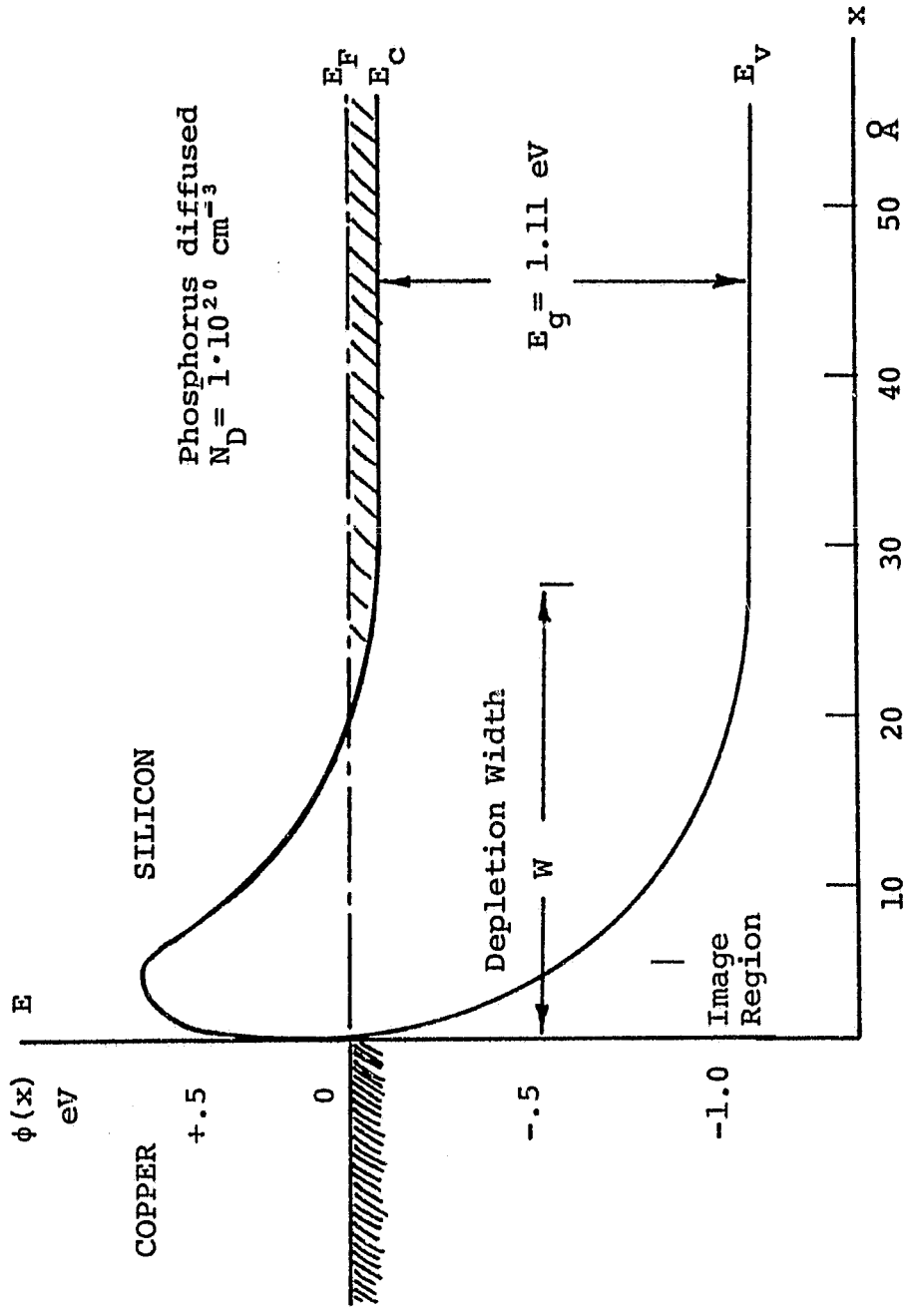


Figure 30 Energy level diagram of copper contact to front of silicon solar cell.

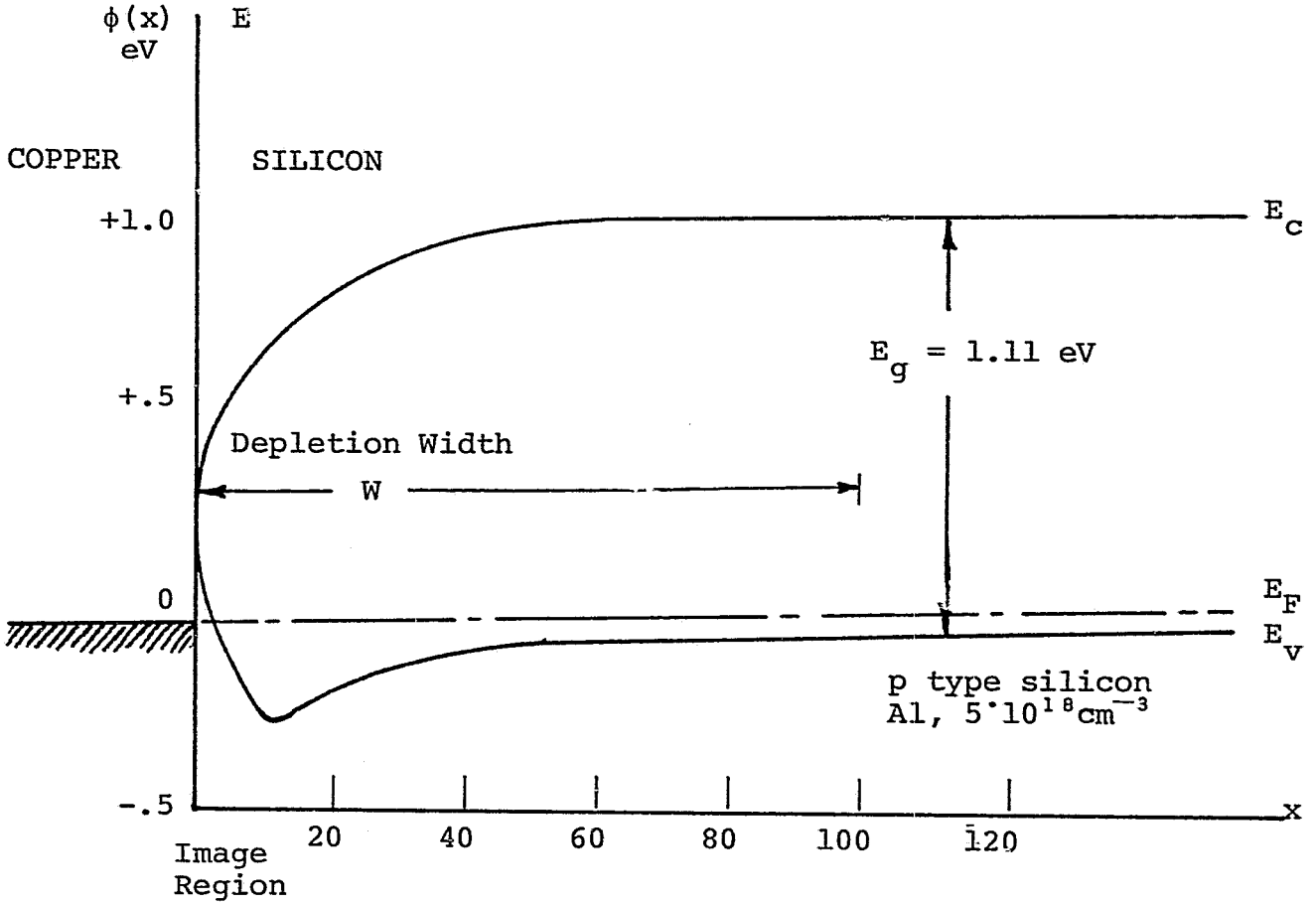


Figure 31 Energy level diagram of aluminum alloy regrowth back contact to solar cell.

metal and allowing it to diffuse into the semiconductor during the firing step, by solid state diffusion. Since only the surface needs to be doped, the donor atom must become a substitutional impurity in the silicon lattice within a few lattice spaces of the surface. A brief firing period will usually suffice.

At very low temperature ( $\lesssim$ 600 C) it may be difficult to obtain a sufficient surface concentration of dopant atoms by diffusion and therefore a different technique is employed. A eutectic alloy of dopant and semiconductor material is made a part of the electrode paste with the object of getting some of the eutectic to bridge semiconductor and metal. During the firing step the eutectic melts, dissolving more silicon. As the temperature is lowered again the dissolved silicon precipitates on the surface, retaining donor solid solubility concentrations, and thereby facilitating ohmic contact. Since the solid solubility of some elements in silicon is small, the use of this method is beneficial only when the front surface donor concentration is less than the donor solid solubility.

## 6.2 Experiments

Two pastes were prepared for the front contact experiment. S071 is an undoped copper paste, which should provide the desired contact on phosphorus diffused solar cells, by virtue of the above arguments. A paste was also prepared

to address the second possibility, providing an epitaxial crystalline layer, doped with antimony. This paste was fabricated by producing an eutectic alloy of antimony-germanium, reducing the resulting ingot to powder, and adding the material to the paste (5 wt.%).

## 7.0 Theoretical Considerations of Reactions

The subject process involves the firing, in special atmospheres, and at elevated temperatures, of a multi-component metal powder ink. These conditions favor the occurrence of numerous chemical reactions.

Such reactions are thought to be the cause of observed poor reproducibility of some performance characteristics of the ink despite care taken to control known parameters. One means for gaining an insight to the possible reactions is the analysis of reasonable combinations or disintegrations of materials present and using principles of chemical thermodynamics and kinetics, to evaluate (even if only qualitatively) the probability that such reactions actually take place.

The heat of a reaction is a readily obtained measure of the tendency of a reaction to proceed. Reactions which produce a great deal of heat are much more likely to occur than those which require the absorption of much heat. The development of the enthalpy change of reaction heat arises from the definition of the enthalpy change of a process, viz.

$$\Delta H = \Delta E + \Delta(pV),$$

and the first law of thermodynamics,

$$\Delta E = Q - W = \Delta H - \Delta(pV).$$

In these equations p is the pressure, V is the volume, and $\Delta E$ is the total energy change for a system change in which an amount of heat, Q, is added to the system and an amount of

work W, is removed from the system. In the case of the reactions of interest the process is one which takes place at constant pressure and involves only volume change work. This leads to:

$$\Delta H_r = Q_p - W + \Delta(pV) = Q_p$$

Which is the enthalpy change or "heat of reaction" for a constant pressure process.

Let us now consider the constant pressure combustion of methane where

$$CH_4 + 2O_2 \rightleftarrows CO_2 + 2H_2O$$

The enthalpy change for this reaction is:

$$\Delta H_r = (H_{CO_2} + 2H_{H_2O}) - (H_{CH_4} + 2H_{O2})$$

Where the subscripted values are the enthalpies of the indicated molecules. This is simply the difference between the initial and final system enthalpies. The above relation may also be written as the enthalpy equation,

$$H_{CH_4} + 2H_{O_2} = H_{CO_2} + 2H_{H_2O} - \Delta H_r$$

Conservation of matter concepts allow us to use molecular heats of formation for the subscripted enthalpies because elemental enthalpies cancel (and are given a value of zero when they appear in a reaction) when enthalpy changes are computed. Tables of heats of formation are readily found (Refs. 10, 11,&12) and this fact makes the rough calculation of heats of reaction a fairly simple matter in most cases. The heats of formation for the gaseous molecules of this example are:

$$\Delta H_{CH_4} = 17.9,\ \Delta H_{O_2} = 0.0,\ \Delta H_{CO_2} = -94.1,\ \Delta H_{H_2O} = -57.8$$

These values are for the 25°C formation at one atmosphere of the gaseous molecules (from elements) expressed in kilocalories per gram mole. The reaction heat for the combustion of one mole of methane under these conditions is therefore;

$$\Delta H_r = -94.1 + 2(-57.8) - (-17.9) - 2(0.0) = 191.8 \text{k cal/mole}$$

The reaction represented here is exothermic since $Q_p (=\Delta H_r)$, the heat put into the system, is negative. The corresponding enthalpy equation is:

$$CH_4 + 2O_2 = CO_2 + 2H_2O + 191.8 \text{ k cal/mole}$$

Here the molecular formulas are used to represent the heats of formation to simplify the notation.

The enthalpy change shown is due to the reaction when carried out at room temperature. Since the state of a system is independent of the process path used to reach it, we may derive a correction expression for enthalpy change in a reaction which takes place at a temperature, $T_1$ other than at room temperature, $T_2$.

The room temperature enthalpy of reaction plus the heat needed to bring the products to temperature $T_1$ is;

$$\Delta H_a = \Delta H_r(T_0) + \int_{T_0}^{T_1} C_p^p \, dT$$

Where $C_p^p$ represents the heat capacity of the products. This corrected enthalpy value, $\Delta H_a$, must be the same as the sum of the heat required to bring the reactants to temperature, $T_1$, and the heat of reaction at $T_1$, which is;

$$\Delta H_b = \Delta H_r(T_1) = \int_{T_0}^{T_1} C_p^r \, dT$$

Where $C_p^r$ represents the heat capacity of the reactants. When these are equated ($\Delta H_a = \Delta H_b$) the desired value for the enthalpy of reaction at $T_1$ is obtained by rearrangement and combination of terms. Thus,

$$\Delta H_r\ (T_1) = \Delta H_r(T_0) + \int_{T_0}^{T_1} (C_p^p - C_p^r)\ dT$$

The correction term in the above equation involves heat capacities at constant pressure which are, in general, functions of temperature.

It was implied earlier that the larger the exothermic heat, the greater the tendency for the reaction, as written, to proceed from left to right. We may infer from the discussion of the heat of reaction that strongly endothermic reactions tend to proceed from right to left.

Two factors which may modify or even overide the above considerations are: 1. Reaction activation energy and 2. Mass action effects. Values for the former are obtained from investigations of the kinetics of the reaction. These will not be detailed here. The latter are based on the general observation that reaction rates increase with an increase in the amount or concentration of reactants. When a reaction produces a gas and a condensed molecule so that the gas tends to separate from the other products, the reverse or right-to-left reaction is inhibited by the loss of the gas. This represents a net increase in the left-to-right reaction.

Because activation energy is often an influential factor in

the observed vigor of a particular reaction scheme, available indications of actual reaction or non-reaction take precedence over other considerations. The relation between the heat of reaction, $\Delta H_r$ and the activation energy, $\Delta E_a$, is shown in Figure 32.

The materials and firing conditions for the current ink formulations suggest the following four categories of reactions:

| | |
|---|---|
| I | Fluorocarbon formulation, Nitrogen atmosphere |
| II | Fluorocarbon formulation, Hydrogen atmosphere |
| III | Silver fluoride, Nitrogen atmosphere |
| IV | Silver fluoride, Hydrogen atmosphere |

In addition to those already indicated, materials of interest are: copper, lead, silicon, silver, and their hydrides, oxides, fluorides, and nitrides. Heats of formation for some of these materials are listed in Table III.

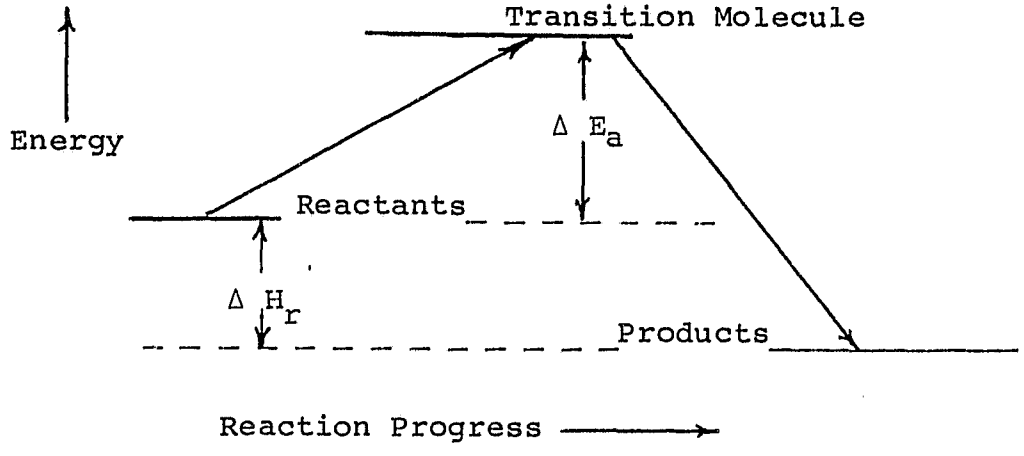


$H_r$ = Heat of Reaction
$E_a$ = Activation Energy

Figure 32 The Relation Between Heat of Reaction and Reaction Activation Energy

TABLE III

Selected Heats of Formation

| Molecule or Atom | State | $\Delta H_f$ 25°C Kcal/mole | Molecule or Atom | State | $\Delta H_f$ 25°C Kcal/mole |
|---|---|---|---|---|---|
| Si | s | 0.0 | $O_2$ | g | 0.0 |
| $SiO_2$ | s | -205.4 | O | g | 59.2 |
| $SiF_4$ | g | -370.0 | CO | g | -26.4 |
| $Si_3N_4$ | s | -179.3 | $CO_2$ | g | -94.1 |
| $SiH_4$ | g | -14.8 | $CH_4$ | g | -17.9 |
| SiC | s | -26.7 | $C_2F_4$ | g | -173.8 |
| | | | $C_2H_4F$ | g | -309.9 |
| Ag | s | 0.0 | | | |
| AgF | s | -48.5 | Cu | s | 0.0 |
| | | | CuO | s | -37.1 |
| F | g | 0.0 | $CuF_2$ | s | -136.9 |
| $F_2$ | g | 18.3 | $CuAc_2$ | s | -213.2 |
| $F_2O$ | g | 5.5 | | | |
| | | | Pb | s | 0.0 |
| $N_2$ | g | 0.0 | PbO | s | -52.2 |
| N | g | 85.6 | $PbO_2$ | s | -66.1 |
| $NF_3$ | g | -11.0 | $PbF_3$ | s | -158.5 |
| $NH_4F$ | s | -111.6 | $PbF_4$ | s | -222.3 |
| | | | $PbAc_2$ | s | -230.5 |
| $H_2$ | g | 0.0 | $PbAc_2.3H_2O$ | s | -443.1 |
| H | g | | | | |
| $H_2O$ | g | -57.8 | $AlF_3$ | s | 311.0 |
| HF | g | -64.2 | | | |

Enthalpy equations for selected category I reactions are:

1. $C_2F_4(g)+SiO_2(s)=SiF_4(g)+2CO(g)+ 43.6$
2. $3C_2F_4(g)+Si_3N_4(s)=3SiF_4(g)+6C(s)+2N\ (g)+ 136.4$
3. $C_2F_4(g)+3Si(s)=SiF_4(g)+2SiC(s)+ 249.6$
4. $C_2F_4(g)+Si(s)=SiF_4(g)+2C(s)+ 196.2$
5. $C_2F_4(g)+2PbO(s)=2PbF_2(s)+2CO(g)+ 91.6$
6. $C_2F_4(g)+2CuO(s)=2CuF_2(s)+2CO(g)+ 58.6$
7. $2N_2(g)+3Si(s)=Si_3N_4(s)+ 179.3$

This selection of "reasonable combinations" is a first pass rather than a complete list. Further analysis should eliminate some listed equations and add some new ones.

It should be noted that the specification of the state of a molecule is important in the choice of a value for its heat of formation. In these (and following) equations, the state, s=solid, g=gas, parenthetically follows the molecular symbol. The above reaction heats (except for equations 2 and 7 ) are for one mole of tetrafluoroethylene.

Although the reaction postulated for the formation of SiC (#3) seems highly favored by a large exotherm and by mass action, it is not observed and therefore equation #3 must be discounted. On the other hand, it is observed that Si is quite likely to react with strongly electronegative atoms so equations #4 and #7 seem reasonable in view of their appreciable exothermic heats.

The rejection of equation #3 is more readily seen when it is

viewed as the sum of two equations, namely, equation #4 and (two times) equation #8 below.

8. $Si(s)+C(s)=SiC(s)+ 26.7$

This reaction has neither a large exotherm nor mass action to favor it.

Reaction #1, which removes $SiO_2$ from the substrate surface is the intended purpose of the fluorocarbon powder in the ink formulation. The occurence of this reaction is supported by some experimental work [12].

None of the other reactions indicated above is particularly beneficial to the ink firing process. Equation #7 suggests the possibility of reaction between nitrogen and fresh silicon surfaces and thereby implies that air-exposed silicon surfaces might be at least partly covered by nitride molecules.

Equations #2 and #4 are strongly favored and specify carbon deposition at the silicon surface due to fluorocarbon reactions. Relatively poor conductivity and adhesion are expected at such sites so reducing the amount of fluorocarbon in formulations should improve ink results.

There are relatively large amounts of copper in these ink formulations so a small amount of copper fluoride formation from equation #6 should cause little trouble but there are only small amounts of formulation lead so equation #5 which converts lead to its fluoride might substantially reduce the proportion of metallic lead and this would suppress the lead-dependent process of liquid phase sintering. Poor

sintering had been noted in fired inks so new formulations appeared to provide improved sintering and adhesion

It is known that there were air leaks into the kiln during earlier experimental ink firings. Some of the likely oxygen reactions are:

9. $Si(s)+O_2(g)=SiO_2(s)+ 205.4$
10. $Cu(s)=1/2O_2(g)=CuO(s)+ 37.1$
11. $Pb(s)+1/2O_2(g)=PbO(s)+ 52.2$

Depending upon where in the process such reactions occurred, the oxides formed could cause poor sintering, poor adhesion, and poor solderability of the fired inks. Appropriate improvements have been made in the process and equipment so that problems due to oxide formation have been all but eliminated.

In the case of category III reactions, where silver fluoride is a constituent of the ink formulation and nitrogen is the firing atmosphere, the equations for selected reactions are:

12. $AgF(s)=Ag(s)+1/2F_2(g)- 48.5$
13. $SiO_2(s)+4AgF(s)=SiF_4(g)+4Ag(s)+O_2(g)- 29.4$
14. $Si(s)+4AgF(s)=SiF_4(g)+4Ag(s)+ 176.0$
15. $Si_3N_4(s)+12AgF(s)=3SiF_4(g)+12Ag(s)+2N_2(g)+ 348.7$
16. $Cu(s)+2AgF(s)=CuF_2(s)+2Ag(s)+ 29.9$
17. $Pb(s)+2AgF(s)=PbF_2(s)+Ag(s)+ 61.5$
18. $CuO(s)+2AgF(s)=CuF_2(s)+1/2O_2(g)+2Ag(s)-7.2$
19. $PbO(s)+2AgF(s)=PbF_2(s)+2Ag(s)+1/2O_2(g)+ 9.3$

Equations #12 and #13 have been previously proposed [13].

Both are endothermic but are aided by mass action. Observation indicates that #12 does not take place to any extent in our firing range of 550 $^{o}$C to 650 $^{o}$C [11], however equation #13 has been shown to proceed [12]. Equation #14 has been observed to take place at an extremely rapid rate [5,6].

Equation #15 appears to be a promising answer to problems arising from silicon nitride formation due to equation #7 since it is strongly favored by exotherm and mass action, and deposits metallic silver rather than carbon which is the residue of fluorocarbon action on silicon nitride (eq. #2).

As in the case of the fluorocarbon reactions, reactions #16 through #19, which produce fluorides of lead and copper are not beneficial to the electrode process. Indeed, the loss of metallic lead through fluoride formation might be quite detrimental. Reductions of silver fluoride content in ink formulations seem to have resulted in improved adhesion and sintering.

Equations for some reactions which might occur during the hydrogen atmosphere portion of the firing, i.e. categories II and IV, are as follows:

20. $CuO(s)+H_2(g)=Cu(s)+H_2O+20.7$

21. $PbO(s)+H_2(g)=Pb(s)+H_2O(g)+5.6$

22. $CuF_2(s)+H_2(g)=Cu(s)+2HF(g)+1.5$

23. $PbF_2(s)+H_2(g)=Pb(s)+2HF(g)-30.1$

24. $SiO_2(s)+4H_2(g)=SiH_4(g)+2H_2O(g)-75.0$

25. $O_2(g)+2H_2(g)=2H_2O(g)+115.6$

26. $Si(s)+2H_2(g) = SiH_4(g) + 14.8$

27. $C(s)+2H_2(g) = CH_4(g) + 17.9$

28. $C_2F_4(g)+H_2(g) = C_2H_2F_4(g) + 136.1$

29. $AgF(s)+1/2H_2(g) = Ag(s)+HF(g) + 15.7$

The reaction heats here are in kilocalories for one gram mole of the first molecule in the equation.

Equations #20 through #23 represent the restoration (by reduction) of metallic copper and lead from their oxides and fluorides which formed during the earlier nitrogen atmosphere portion of the firing cycle. Equation #20 is observed (by color change) to take place under conditions of hydrogen firing, but the endothermic reaction of equation #23 probably does not take place, to any appreciable extent, despite its mass action assist.

The above reductions and their reverses (oxidations) could be verified by Thermogravimetric Analysis (TGA) methods. Table IV summarizes the expected TGA results. In these experiments the reverse fluoride reactions would be done in $N_2$ with excess fluorocarbon polymer powder mixed with the metal powder since the fluorocarbon has been found to convert completely to gaseous products above 550°C or so.

Table IV Data for Metals Oxidation and Reduction Studies

| Compound | Color | MW | Metal MW | React. # | Oxide. % Wt. Gain | Redu. % Wt. Loss |
|---|---|---|---|---|---|---|
| CuO | Black | 79.5 | 63.6 | 20 | 25.0 | 20.0 |
| PbO | yellow | 223.2 | 207.2 | 21 | 7.7 | 7.2 |
| CuF | white | 101.5 | 63.6 | 22 | 59.6 | 37.3 |
| PbF | color-less | 245.2 | 207.2 | 23 | 18.3 | 15.5 |

The indirect evidence that reductions of fluoride in ink formulations bring improved bonding and sintering supports the idea that equation #23 does not proceed and that once lead fluoride is formed, it remains in the fired ink.

It is well known that the endothermic reaction of eq. #24 does not take place even at the elevated temperatures of ink firing. Equation #25 has been observed (by moisture condensation) at firing temperatures, but the extent of the equation #26 reaction may be limited because of the instability of many of the silanes.

Equation #26 may be more accurately stated by:

$$nSi+(n+1)H_2 \rightleftarrows Si_nH_{2n+2}$$

Similarly, the reaction of equation #27 could be written,

$$nC+(n+1)H_2 \rightleftarrows C_nH_{2n+2}$$

The heats of formation per mole of carbon (or silicon) hydrides decrease asymptotically with increasing n, as shown in Figure 33.

This indicates that the n=1 compounds would strongly

predominate in the composition of a reaction mix.

The classic procedure for the production of silanes using magnesium silicide in $H_2$ and HCl[16] results in 40% SiH, 30% $Si_2H_6$, 15% $Si_3H_8$, 10% $Si_4H_{10}$ and 5% higher silanes[17].

Non-volatile silicon hydride polymers which include an unsaturated bond have also been prepared[17]. These may arise from,

$$nSi + nH_2 \rightleftarrows (SiH_2)_n$$

Condensed hydride polymers or homologues of silicon (silanes) or carbon (alkanes) deposited on the silicon substrate would be expected to affect adversely the physical and electrical properties of fired inks.

On examination of the reaction enthalpies and mass action effects it appears likely that hydrogen does react, during firing, with residual tetrafluoroethylene (eq. #28) in category II or with silver fluoride (eq. #29) in category IV.

The hydrogen atmosphere phase of firing has been associated with frequent random incidents of very poor ink adhesion using inks which previously gave excellent bonding. In some cases, ink samples which were well bonded (but somewhat oxidized) during the nitrogen firing showed no bonding after hydrogen firing. One possible explanation is that bonding sites on the silicon substrate are chemically attacked by the HF generated according to equations #22 and #29 in hydrogen firing.

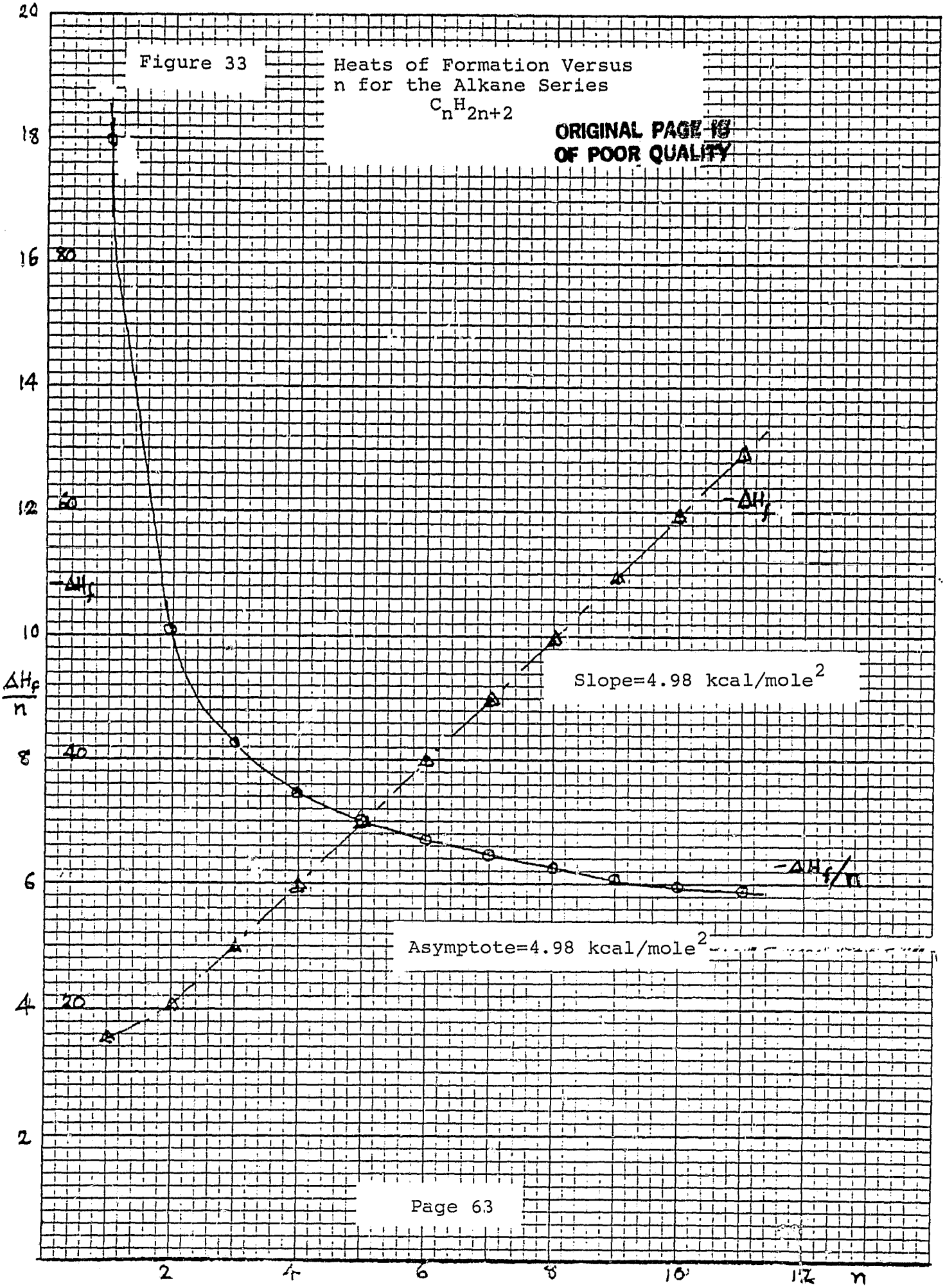
Figure 33
Heats of Formation Versus n for the Alkane Series $C_nH_{2n+2}$
ORIGINAL PAGE IS OF POOR QUALITY
$-\Delta H_f$
$-\frac{\Delta H_f}{n}$
Slope=4.98 kcal/mole$^2$
Asymptote=4.98 kcal/mole$^2$
$-\Delta H_f/n$
n
20
18
16
14
12
10
8
6
4
2
80
60
40
20
2
4
6
8
10
12

A reduction of the temperature of the ink sample during hydrogen firing gives an improvement in ink bonding, which could be attributed to a reduction in the extent of equations #22 and #29.

Another hypothesis is the occupation of dangling electron bonds on silicon surfaces by hydrogen or possibly the displacement of metal atoms by hydrogen (section 8.0). These preliminary applications of simple chemical ideas have pointed to some fruitful directions for experimental work aimed at improvement of ink materials and processes. In particular, progressive fluoride reductions and milder hydrogen treatments, which were suggested by thermochemical and mass action considerations, proved quite beneficial to the mechanical properties of the ink system.

Inconsistency of results still plagues the ink formulations containing fluorocarbon powder, and early studies of ink electrical performance indicate a need for increased knowledge of the chemistry of these ink systems.

To this end, the work of this report should be expanded to include literature searches to unearth more possible reactions and provide needed heat capacities and activation energies. Experimental work making use of TGA and differential thermal analysis (DTA) should be increased and in addition, the simple theoretical tools of chemical kinetics and chemical equilibrium should be applied to the determination of the likely extent of candidate reactions.

## 8.0 Information Exchange with German R&D Labs

During the month of October, two Siemens facilities in Munich, Germany were visited. At the semiconductor device plant at Frankfurter Ring, Drs. K. Reuschel and K. Platzöder were met and device processing was discussed.

The Wacker-Chemie plant at Burghausen, Bavaria, Mr. Vieweg-Gutberlet was also visited and silicon material properties (minority carrier lifetime and defect phenomena) were discussed.

The Solid State Institute (IFT) of the Fraunhofer-Gesellschaft was visited and contact problems, as well as minority carrier lifetime measurements were discussed with Dr. H. Sigmund.

Siemens Research Labs, Neu-Perlach was visited on two occasions and solar cell research (Siemens' amorphous sputtering and evaporation approach) were discussed, as well as contact problems, minority carrier lifetime measurement and other activities. Research lab personnel interviewed were Drs. G. Winstel, J.G. Grabmaier, E.F. Krimmel, Patalong, M. Möller, R.D. Plättner and Herberg.

Several papers were obtained from the Siemens group. One of these discussed the strong attachment of hydrogen to the dangling bonds in amorphous silicon material. Quoting the reference "The most striking feature shown by these measurements is however the great bond strength of the hydrogen in the a-Si:H,Cl network up to very high temperatures. Only at temperatures of about $1000^0$K do perceptible

amounts of hydrogen escape, which may be due to recrystallization setting in at this temperature[18]. Since the surface of crystalline silicon has dangling bonds, similar to the amorphous material, this may help explain the displacement of silver and copper observed at high temperatures in hydrogen ambients. This phenomenon is discussed in further detail in the appropriate section.

## 9.0 Firing Experiments

### 9.1 Furnace Calibration

Evidence of drifting of the temperature control Chromel-Alumel thermocouple led to a recalibration of the furnace. The profile shown in figure 34 resulted from probing the furnace tube with a Pt - Pt + 13% Rh thermocouple connected to a digital microvolt meter. Only the exit portion of the profile extending beyond the center of the furnace is shown, as it is the region of major interest in our experimentation.

It has been made a part of the experimental protocol to get temperature readings at least at the beginning and end of each run with the platinum thermocouple and digital meter.

FIGURE 34 'TUBE FURNACE PROFILE

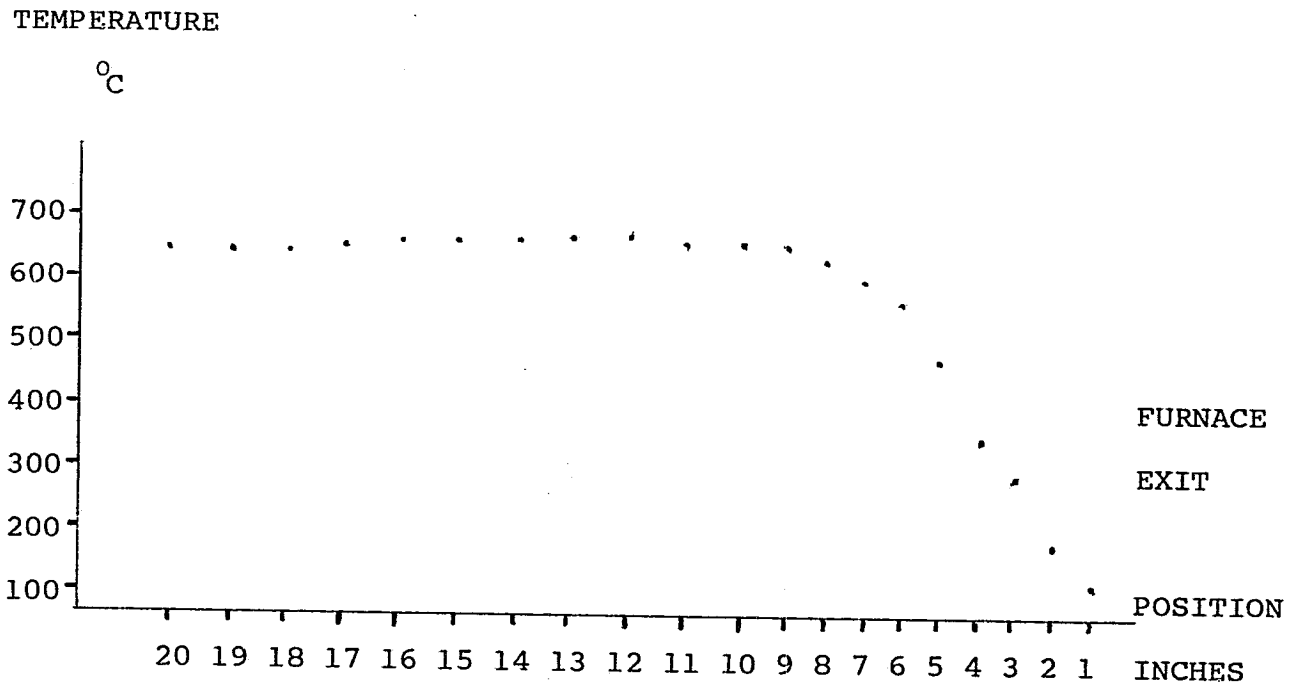

## 9.2 Gas Ambients

During firing tests it was found that:

a) nitrogen firing resulted in severely oxidized copper grains

b) the position of silicon wafers (standing in slotted boat or lying flat) had a bearing on the results

c) the duration of the second step (hydrogen flow) in the two step firing was a factor in the adherence of the electrode to the silicon substrate

Several explanations are possible for this behavior. Contamination of the source flow gases was ruled out, since it was verified that all nitrogen procured, since firing first commenced, was oil pumped (vs. water pumped), and no other evidence pointed in that direction. However back streaming, convective flow and therefore air contamination of furnace atmosphere in the open exit quartz tube was considered likely. Further, contamination of furnace quartz furniture was a possibility and was therefore assumed. The following steps were taken at the end of the reporting period to counter the reported problems.

1) Convection and backstreaming were reduced by insertion of an alumina "wool" plug into the quartz tube exit during firing. This plug restricts the exit diameter, breaks up the gas stream into a number of small filamentary streams and increases the velocity of the streams markedly, thereby reducing backdiffusion.

2) All quartz furniture was taken to a professional glass shop for cleaning.

During the final portion of the reporting period it was found that the higher the temperature of the hydrogen treatment, the more likely electrode separation would occur. At temperatures below 380 $^{0}$ C, the effect of hydrogen upon adhesion appeared to be minimal. For this reason a firing profile was devised as shown in figure 35 While there was some concern that initial oxidation might impair the frit metal wetting process of the copper grains, this proved to be a less significant factor for the following reason: During the initial firing process a reducing atmosphere is produced in the furnace by the organic constituants of the paste vehicle and binder. This material is removed and transported away from the firing site. Only then does the coppergrain matrix as well as the lead frit metal become succeptible to oxidation due to contamination, backstreaming and backdiffusion of oxygen. While this can be reduced, as discussed in the next section, the use of hydrogen during the cooling phase of the firing cycle is helpful in maintaining metallic surface properties and appearance.

Figure 35 MODIFIED FIRING PROFILE

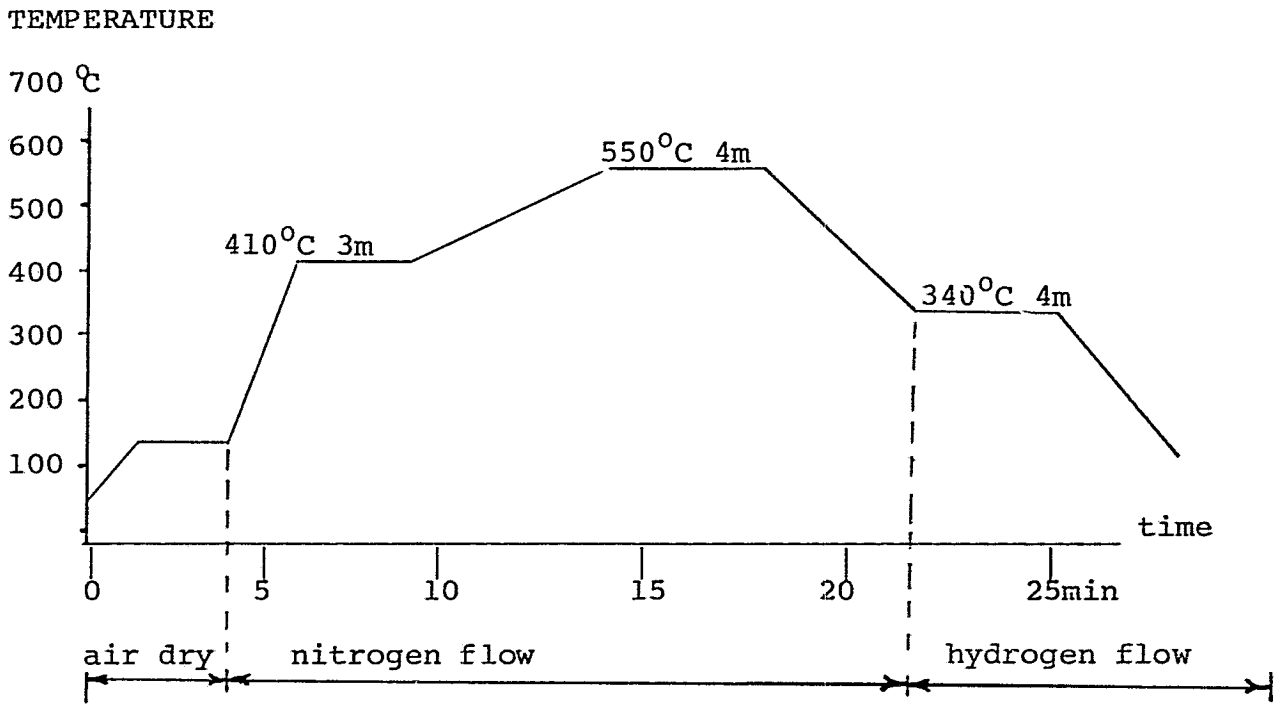

.0 Firing Experiments (cont.)

.3 Cleaning Procedure

1) Bakeout at 570°C in air (burnout of organic chemicals, convert metals to oxide, remove strains in quartz)
2) Soak in 30% hydrofluoric acid
3) Scrub with cheesecloth (in dilute hydrofluoric acid)
4) Rinse in deionized water and dry

This cleaning procedure is routinely used by General Atomics Corportation, San Diego.

A number of firing experiments were done after the furnace quartz ware was returned to service. The exit baffle diffuser plug allowed making pure nitrogen flow firing without showing visible oxidation. However, neither sintering activity nor adherence were significantly improved. Further the reproducibility of results with specific pastes either in separate firings or one firing experiments are done in a semi-closed system, it was felt that relocation of the equipment might be beneficial. The location of the firing equipment until June 1981, approximately two miles from the Pacific Ocean coast, is within marine layer weather influence. Of particular concern is the possible major contamination with aerosol salt powders. Some evidence of this was seen in the sodium yellow flicker of the hydrogen effluent of the exit flame curtain. It was therefore decided to relocate the firing

facility to the Electrink plant approximately 9 miles from the Pacific coast and more under desert weather influence.

## 10.0 Preliminary Cost Analysis

While pastes manufactured to date do not satisfy all the requirements with respect to adhesion, electrical properties and resistance to environmental factors, a preliminary cost study was undertaken.

The cost elements provided in this study should be looked upon as constituting the upper limit in most cases. The major constituent, copper metal powder, is presently obtained from a high priced source in order to maintain close limits on a variety of physical parameters. It is expected that further experimentation and insight will allow the utilization of a less expensive material, however, present calculations are based upon the high copper price of $32/lb.. This material has not been made in volume production by the manufacturer.

The sample pastes chosen for the cost analysis are F12 (silver fluoride) and F13 (fluorocarbon) composition. Material costs and component cost percentages are given in Table V. The material costs are given in dollars per troy ounce of paste.

The third and sixth column of numbers give the component cost percentages of the total paste material costs. This number shows the cost drivers which are (in order of importance): copper, solvent, resin and eutectic materials, with silver fluoride being in 5th place.

TABLE V Cost of Materials of Fluorocarbon and Silver Fluoride Activated Copper Pastes

| | PASTE F12 | | | PASTE F13 | | |
|---|---|---|---|---|---|---|
| MATERIAL | AMOUNT(wt%) | COST $ | COST % | AMOUNT(wt%) | COST $ | COST % |
| Organic Solvent | 31.2 | 0.343 | 20.5 | 30.8 | 0.338 | 21.0 |
| Resin | 4.2 | 0.093 | 5.56 | 2.2 | 0.0619 | 3.83 |
| Thixotropic Agent | 0.6 | 0.0089 | 0.53 | 0.4 | 0.0059 | 0.37 |
| Copper Powder | 57.1 | 1.142 | 68.29 | 56.9 | 1.138 | 70.44 |
| Lead Powder | 4.6 | 0.014 | 0.84 | 4.6 | 0.014 | 0.87 |
| Aluminum-Silicon Eutectic | 1.2 | 0.044 | 2.63 | 1.1 | 0.041 | 2.54 |
| Silver Fluoride | 1.1 | 0.0275 | 1.64 | - | - | - |
| Lead Acetate | - | - | - | 2.3 | 0.0122 | 0.76 |
| FluoroCarbon | - | - | - | 1.1 | 0.0043 | 0.27 |
| TOTAL MATERIAL COST | | $1.6724/oz | | | $1.6156/oz | |

Based upon moderately large quantity production, the labor has been calculated at $0.50 per oz.

| | | |
|---|---|---|
| Labor + Material | $2.1724/oz | $2.1156/oz |

Depreciation:

The major apparatus for paste fabrication is the roller mill. New cost for a 5 X 10" mill is $8,000. Assuming an eight year life, milling rate of 12 oz/hour, 24,000 oz/year or 200,000 oz/per mill life. Factoring this into purchase costs gives $0.04/ oz depreciation cost.

F12 = $2.2124/ oz  F13 = $2.1556/ oz

Ancillary Material Costs

Paper wipes: one per oz , 140/box @ $2.00/Box, $0.014/oz

Cleaning solvent (MEK) $209.60/55 gal. drum

= $3.8/ gal

$1.007/liter and 50cc/oz $0.050/oz

Glassware (breakage + packaging)

| | | | |
|---|---|---|---|
| 1 beaker/1000 oz | @ $2.00 | $.002 | |
| 10 oz jar | @ $0.45 | $.045 | $0.047/oz |
| | | | $0.111/oz |

F12 = $2.3234/oz  F13 = $2.2666/oz

Postulating a yield of 80%

| F12 | F13 |
|---|---|
| $2.904/ oz | $2.833/ oz |

and stipulating a gross profit and sales cost of 30% we h
a final cost of

| | |
|---|---|
| S3.77/ oz(silver fluoride) | S3.68/ oz(fluorocarbon) |
| $0.121/g | $0.118/g |

Cost per cell (Assuming 4" OD)

| | | |
|---|---|---|
| Front | 8% coverage | 0.025g required |
| Back | 95% | 0.297g required |
| | Total | 0.322g required |

| | |
|---|---|
| $0.0390/cell | $.0380/cell |

Additional cost of hydrogen firing: $60/1000 cu. ft.
flow 5 l /min for 30 min./run 28,300 l/tank = 189
runs/tank

50 cells/run 189 runs = 9450 cells/tank @ $60

$60/tank / 4450 cells = $0.0063/cell

Contact cost per cell

| | F12 (silver fluoride) | F13 (fluorocarbon) |
|---|---|---|
| | $0.0390/cell | $0.0380/cell |
| hydrogen cost | .006 | .006 |
| | $0.0450/cell | $0.0440/cell |

## 11.0 Conclusions and Problems

1. Both silver-fluoride and fluorocarbon screened paste electrodes can be produced for approximately $0.04 per watt.
2. Reproducible results have been achieved with adherent copper electrodes containing 0.7 wt.% silver-fluoride, although size of the firing load may be a factor.
3. Analogous results with amorphous silicon support the hypothesis that hydrogen replaces metal - silicon bonds. This led to a modified two step firing process.
4. A non optimum fluorocarbon activated copper paste (F16) gave a projected AM 1 efficiency of 10%.
5. Carbon fluoride-copper pastes require further modification to achieve reproducibly adherent electrodes.

## 12.0 Recomendations

A problem which must be solved is the lack of reproducibility. This may be due in part to the variability in certain raw materials such as silver fluoride, and to the possibility of self contamination, possibly based upon the number of wafers being fired.

A more complete understanding of the chemical processes, outlined in Section 7, would be helpful in achieving better control. This can be facilitated by further experiments with thermogravimetric analysis (TGA) and differential thermal analysis. (DTA)

The role of hydrogen on the silicon surface can only be hypothesized at this point. Further experimentation and analysis with the properties of silicon surfaces exposed to various heat treatments in hydrogen ambients, would be not only helpful to a narrow segment photovoltaic processing technology, but to the whole semiconductor technology and industry.

Another approach to the hydrogen problem is experimentation with alternative reducing ambients, such as carbon monoxide for example.

Finally the question whether copper electrodes can be used in solar cell front surfaces must be further addressed.

## 13.0 New Technology

No new technology of patentable nature was developed during the present term of this contract.

14.0 PROGRESS ON PROGRAM PLAN

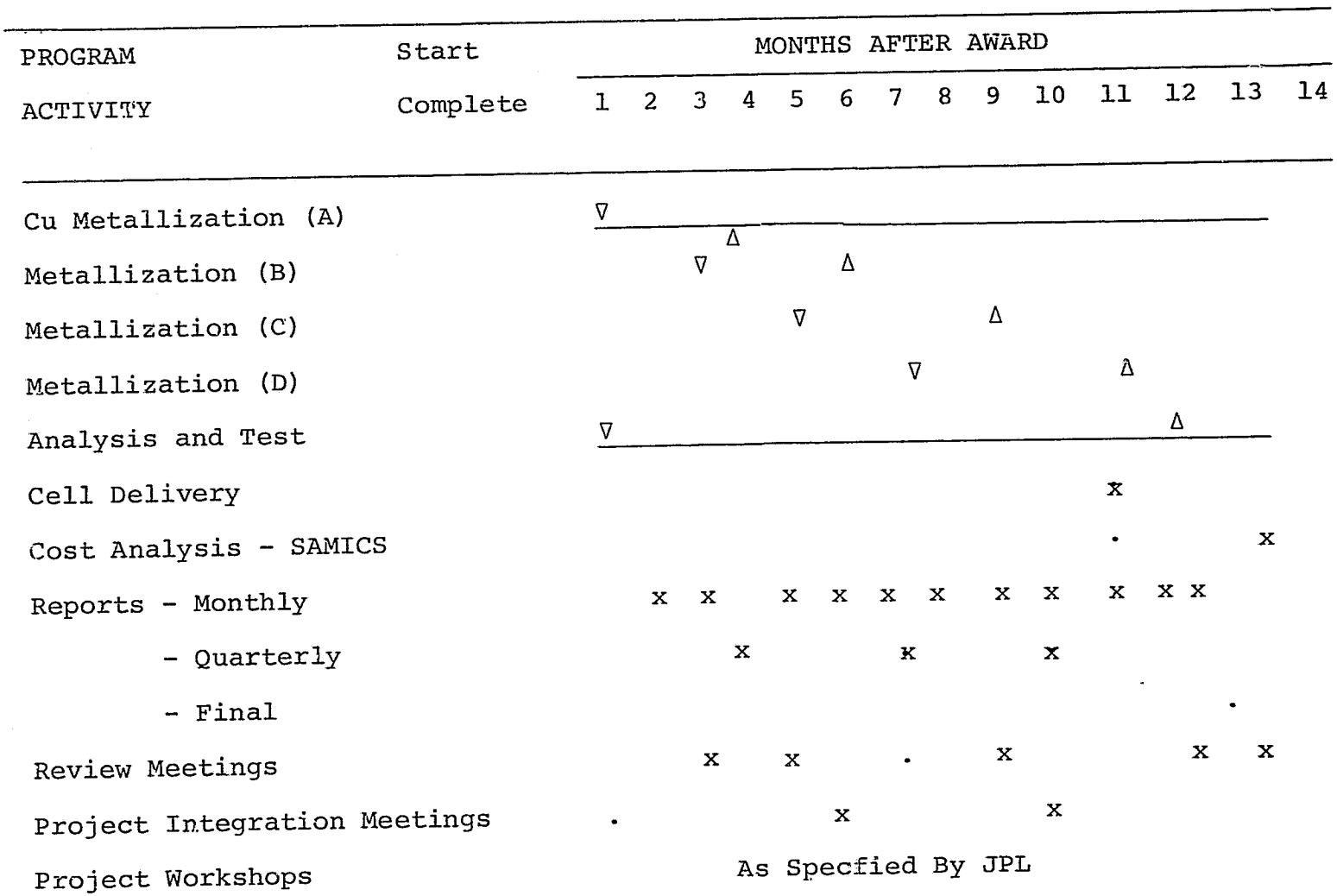

## 15.0 Appendix

TABLE VI

PASTE COMPOSITIONS (wt %)

| Code | Vehicle | Cu metal | Oxide Scavenger | Lead Frit metal | Lead Acetate | Eutectic Additive |
|---|---|---|---|---|---|---|
| F1 | | | | | | |
| 2 | Similar to S071 | | Different suppliers | | | |
| 3 | 23 | 69.3 | A3.9 | 3.9 | - | - |
| 4 | | | | | | |
| 5 | 23 | 70 | C1.6 | 5 | - | - |
| 6 | 44 | 49.8 | | A3.1 | - | - |
| 7 | 43 | 52 | C1.2 | 3.5 | - | - |
| 8 | 35.3 | 60 | C1.2 | 3.5 | - | G3.9 |
| 9 | 22.2 | 66.7 | A3.7 | 3.7 | - | G3.7 |
| 10 | 22 | 66.6 | A3.7 | 3.8 | - | - |
| 11 | 36 | 53.3 | C2.1 | 4.3 | - | S4.3 |
| 12 | 36 | 57.1 | A1.1 | 4.6 | - | S1.2 |
| 13 | 34 | 56.9 | C1.1 | 4.6 | 2.3 | S1.1 |
| 14 | 33 | F57.8 | C1.1 | 4.6 | 2.3 | S1.2 |
| 15 | 43.4 | F48.8 | C0.9 | 3.9 | 2.0 | S1.0 |
| 16 | 33 | 55.8 | C1.1 | 4.5 | 4.5 | S1.1 |
| 17 | 33 | 58.8 | A1.2 | 5.9 | - | S1.1 |
| 18 | 32 | 57.7 | C1.1 | 5.8 | 2.3 | S1.1 |
| 19 | 31 | 59.4 | C0.7 | 5.9 | 2.4 | S0.6 |
| 20 | 30 | 62.4 | A0.7 | 6.2 | - | S0.7 |
| 21 | 28 | 61.2 | A3.6 | 3.6 | 1.5 | - |
| 22 | 34 | 55.8 | C1.1 | sn 3.6<br>Pb 1.5 | 4.5 | - |

F = Flake  C = Fluorocarbon  G = Al-Ge
A = Silver Fluoride  S = Al-Si

## 16.0 References

1. B. Ross, Proceedings of the 14th IEEE Photovoltaic Specialists Conference, San Diego, CA, p. 787

2. B. Ross, Proceedings of the 14th IEEE Photovoltaic Specialists Conference, San Diego, CA, p. 1406

3. B. Ross, Extension Final Report "Production Process and Equipment Development" DOE/JPL 955164 - 79/4 p. 72 (Dec. 1979)

4. B. Ross, Quarterly Report #3 "Development of an All-Metal Thick Film Cost Effective Metalization System for Solar Cells" DOE/JPL 955688 - 80/7, p. 18 (Sept. 1981)

5. Loc cit, Ref. 3, p.10

6. Ibid, p. 72

7. M.P. Lepselter and J. M. Andrews in Ohmic "Contacts to Semiconductors", B. Schwartz, Ed., Electrochem. Soc. p. 159 New York (1969)

8. E.H. Rhoderick, "Metal Semiconductor Contacts", Clarendon Press, p. 59, Oxford (1978)

9. J.G Simmons, Jour. Appl. Phys., 34 1793 (Jun 1973)

10. Handbook of Chemistry and Physics, 57th edition, CRC Press, Cleveland, OH, (1976-77)

11. F.T. Wall, "Chemical Thermodynamics", W.H. Freeman, San Francisco, CA, p. 47 et seq. (1958)

12. B. Ross, and D. Mentley Quarterly Report #1 "Development of Economical Improved Thick Film Solar Cell Contacts", DOE/JPL 955-164-78/4 p. 9,10 (Jan. 1979)

13. B.H. Mahan, "Elementary Chemical Thermodynamics", W.A. Benjamin, New York, N.Y., p. 27-36 (1963)

14. N.I. Sax, "Dangerous Properties of Industrial Materials", Van Nostrand-Reinhold, New York, p. 972. (1979)

15. L. Bretherick, "Handbook of Reactive Chemical Hazards", Butterworths, London, P. 197. (1979)

16. A. Stock, "Hydrides of Boron and Silicon", Cornell Univ. Press, Ithica, N.Y., (1933).

17. T. Moeller, "Inorganic Chemistry", John Wiley, New York, (1952)

18. R.D. Plättner, W.W. Kröhler, B. Rauschen, W. Stetter and J.G. Grabmaier., Proc. 2nd E.C. Photovoltaic Solar Energy Conference, p. 860, Berlin W. (Apr. 1979)